Development/Plasticity/Repair

Mesoscale Architecture Shapes Initiation and Richness of Spontaneous Network Activity

Samora Okujeni,[1,2] Steffen Kandler,[1,2] and Ulrich Egert[1,2]

[1]Bernstein Center Freiburg and [2]Biomicrotechnology, IMTEK—Department of Microsystems Engineering, University of Freiburg, 79110 Freiburg, Germany

Spontaneous activity in the absence of external input, including propagating waves of activity, is a robust feature of neuronal networks *in vivo* and *in vitro*. The neurophysiological and anatomical requirements for initiation and persistence of such activity, however, are poorly understood, as is their role in the function of neuronal networks. Computational network studies indicate that clustered connectivity may foster the generation, maintenance, and richness of spontaneous activity. Since this mesoscale architecture cannot be systematically modified in intact tissue, testing these predictions is impracticable *in vivo*. Here, we investigate how the mesoscale structure shapes spontaneous activity in generic networks of rat cortical neurons *in vitro*. In these networks, neurons spontaneously arrange into local clusters with high neurite density and form fasciculating long-range axons. We modified this structure by modulation of protein kinase C, an enzyme regulating neurite growth and cell migration. Inhibition of protein kinase C reduced neuronal aggregation and fasciculation of axons, i.e., promoted uniform architecture. Conversely, activation of protein kinase C promoted aggregation of neurons into clusters, local connectivity, and bundling of long-range axons. Supporting predictions from theory, clustered networks were more spontaneously active and generated diverse activity patterns. Neurons within clusters received stronger synaptic inputs and displayed increased membrane potential fluctuations. Intensified clustering promoted the initiation of synchronous bursting events but entailed incomplete network recruitment. Moderately clustered networks appear optimal for initiation and propagation of diverse patterns of activity. Our findings support a crucial role of the mesoscale architectures in the regulation of spontaneous activity dynamics.

Key words: **clustering; network structure; neuronal networks; protein kinase C; spatiotemporal pattern; spontaneous activity**

Significance Statement

Computational studies predict richer and persisting spatiotemporal patterns of spontaneous activity in neuronal networks with neuron clustering. To test this, we created networks of varying architecture *in vitro*. Supporting these predictions, the generation and spatiotemporal patterns of propagation were most variable in networks with intermediate clustering and lowest in uniform networks. Grid-like clustering, on the other hand, facilitated spontaneous activity but led to degenerating patterns of propagation. Neurons outside clusters had weaker synaptic input than neurons within clusters, in which increased membrane potential fluctuations facilitated the initiation of synchronized spike activity. Our results thus show that the intermediate level organization of neuronal networks strongly influences the dynamics of their activity.

Introduction

A remarkable feature of neocortical circuitry is the generation of rich spontaneous activity dynamics (Sanchez-Vives and McCormick, 2000; Logothetis et al., 2009; Yanagawa and Mogi, 2009; Sato et al., 2012), which are believed to play an important role in cortical processing and development (Shatz, 1996; Wu et al., 2008; Ringach, 2009; Kilb et al., 2011; Altwegg-Boussac et al., 2014).

Computational network models predict that modular network architectures with highly intrinsically connected subnetworks (i.e., clustered networks) are optimal in generating and sustaining network activity (Kaiser and Hilgetag, 2010; Klinshov et al., 2014) and promote firing-rate variability and state transitions (Litwin-Kumar and Doiron, 2012).

In a simplified view, cortical neurons are indeed arranged in local clusters that have high intrinsic connectivity and connect to other clusters by correlated long-range patchy projections, i.e.,

Received Aug. 11, 2016; revised Feb. 6, 2017; accepted Feb. 11, 2017.

Author contributions: S.O. and U.E. designed research; S.O. and S.K. performed research; S.O. analyzed data; S.O. and U.E. wrote the paper.

This work was supported by BrainLinks-BrainTools, Cluster of Excellence funded by the German Research Foundation (Grant EXC 1086), and Bernstein Focus: Neurotechnology Freiburg–Tuebingen (FKZ 01GQ0420). We thank Sarah Jarvis, Ehsan Safavieh, and Oliver Weihberger for helpful discussions and gratefully acknowledge technical assistance from Ute Riede, Patrick Pauli, Alexander Giffey, Hanna Kuhn, Nila Mönig, and Patrick Ringwald.

Correspondence should be addressed to Samora Okujeni at the above address. E-mail: okujeni@bcf.uni-freiburg.de.

S. Kandler's present address: Neuro-Electronics Research Flanders, Imec Campus, Leuven, Belgium.

DOI:10.1523/JNEUROSCI.2552-16.2017

 0270-6474/17/373972-16$15.00/0

neurons in a cluster share common long-range target regions (Ruthazer and Stryker, 1996; Voges et al., 2010). Functionally, this has been linked to the association of neuronal ensembles with similar function, for example the representation of orientation selectivity in the visual cortex (Bosking et al., 1997; Chavane et al., 2011). However, implications of this mesoscale network architecture for spontaneous neuronal dynamics remain speculative.

We tested the theoretical predictions in readily accessible neuronal networks *in vitro* by modifying the spatial distributions of neurons and neurites. In an abstract way, these networks display a mesoscale architecture with some resemblance to that of the cortex. Cultured neurons spontaneously aggregate to form clusters and grow fasciculated neurites connecting them (Kriegstein and Dichter, 1983; Segev et al., 2003; Robert et al., 2012). Their functional clustering is revealed by the spatial fragmentation of the networks when excitatory synaptic transmission is diminished (Soriano et al., 2008). Functional network reconstruction likewise indicates a mixture of locally clustered and long-range connectivity (Stetter et al., 2012). These networks establish rich spontaneous dynamics (Marom and Shahaf, 2002; van Pelt et al., 2004; Wagenaar et al., 2006a) consisting of propagating synchronized bursting events (SBEs), which are similar to patterns of spontaneous activity characteristic for the developing neocortex (Katz and Shatz, 1996; Wu et al., 2008; Golshani et al., 2009).

We modified the structure of these networks by pharmacological modulation of protein kinase C (PKC), an enzyme regulating neurite growth (Dent and Meiri, 1998), branching (Quinlan and Halpain, 1996; Audesirk et al., 1997; Schrenk et al., 2002; Gundlfinger et al., 2003; Metzger, 2010), fasciculation (Itoh et al., 1989), and cell migration (Kumada and Komuro, 2004; Larsson, 2006). By exploiting the formative effects of PKC modulation, we made networks with more clustered respectively more uniform (defined as toward randomness) arrangement of neurites and somata. Chronic PKC activation (PKC^+) promoted neuronal aggregation, neurite entanglement in clusters and axonal fasciculation, and reduced overall neurite densities, suggesting more local and less long-range connectivity. Inhibition of PKC (PKC^-) diminished soma clustering and axonal fasciculation and increased neurite densities, suggesting more uniform connectivity.

Differences in the mesoscale architecture crucially affected the generation and spatiotemporal structure of spontaneous activity. In PKC^- networks, spontaneous SBEs were elicited at significantly lower rates even though these networks were highly excitable, as indicated by high responsiveness to electrical stimulation. We suggest that reduced clustering and fasciculation diminished recurrent and convergent connectivity patterns that promote background activity integration and SBE initiation. Neurons in clustered networks and particularly those within clusters indeed received stronger synaptic inputs, increasing membrane potential (V_m) fluctuations. Widely distributed burst initiation zones (BIZs) in clustered networks established a much richer repertoire of propagating waves compared with uniform networks where SBEs were elicited only from a few hotspots. However, clustering also resulted in incomplete network recruitment during SBEs, leading to restricted activation patterns and global desynchronization.

Our results support theoretical predictions that clustered network topologies promote generation, maintenance, and richness of spontaneous activity. A balance between local and long-range connectivity furthermore seems necessary for the generation of spontaneous activity dynamics that recruit large parts of the network at the same time.

Materials and Methods

Cell culture techniques. Primary cortical cell cultures were prepared on different microelectrode arrays (MEAs; Multi Channel Systems; electrode grid layout/pitch distance: 8 × 8/200 μm; 6 × 10/500 μm; 16 × 16/200 μm; 32 × 32/300 μm) and standard coverslips (12 mm diameter, Carl Roth). All substrates were coated with polyethylene-imine (150 μl of 0.2% aqueous solution; Sigma-Aldrich) for cell adhesion. Cell cultures were prepared following Shahaf and Marom (2001). Cortical tissue was prepared from brains of neonatal Wistar rat pups of either sex, minced with a scalpel, and transferred into PBS (Invitrogen). Tissue pieces were incubated with trypsin (isozyme mixture, 0.05%, 15 min at 37°C; Invitrogen) and proteolysis was subsequently stopped with horse serum (20%; Invitrogen). DNase (type IV, 50 μg/ml; Sigma-Aldrich) was added to eliminate cell trapping in DNA strings if needed. Cells were dissociated by trituration with a serological pipette, centrifuged (5 min, 617 × *g*), and resuspended in growth medium [Minimal Essential Medium supplemented with 5% heat-inactivated horse serum, 0.5–1 mM L-glutamine, 20 mM glucose, and 20 μg/ml gentamycin (all from Invitrogen); 1 ml/pup]. Cells were counted with an automated cell counter (CASY, Schärfe Systems) and seeded at 300,000 cells per culture, resulting in a density of 1500 cells/mm^2 at 1 d *in vitro* (DIV). Networks developed in 1 ml of growth medium in a humidified incubator (5% CO_2, 37°C). Animal handling and tissue preparation were done in accordance with the guidelines for animal research at the University of Freiburg.

PKC modulation and disinhibition. PKC inhibitor Gödecke6976 (Gö6976; 1 μM; Sigma-Aldrich) and PKC agonist phorbol-12-myristate-13-acetate (PMA; 1 μM; Sigma-Aldrich) were dissolved in dimethylsulfoxide (DMSO; Sigma-Aldrich) and added to the culture medium directly after cell preparation. The maximal concentration of DMSO in the growth medium was 0.1%. GABAergic transmission was probed by acute application of the noncompetitive $GABA_A$ receptor antagonist picrotoxin (PTX; 10 μM; Sigma-Aldrich) during electrophysiological recordings. Drug washout was performed by a complete medium exchange with fresh medium after ~4 weeks. Networks growing without PKC modulation (PKC^N) were treated the same way to evaluate general washout-induced effects. Cultures were subsequently recorded repeatedly within the next days.

Morphological analyses. Cell adherence after seeding was documented by phase contrast microscopy at 1 DIV to estimate initial cell densities. Cell positions were determined in phase contrast micrographs by automated detection (2D convolution with a Mexican hat-shaped kernel with an inner radius corresponding to the diameter of neuronal cell bodies and subsequent thresholding of the resulting image). The spatial distribution of neuronal cell bodies was reexamined after 21 DIV based on immunocytochemical staining of neuronal nuclei (NeuN; rabbit-anti-NeuN, 1:500; Abcam) and staining of all cellular nuclei (DAPI; Sigma-Aldrich). Cellular nuclei were detected automatically (similar approach as described above) and neurons were identified as the subset of cells with NeuN immunoreactivity.

To assess minimal possible distances between neuronal somata, we calculated the distance between the centers of pairs of neurons by Delaunay triangulation. Spatial clustering of cell bodies was evaluated by a modified Clark–Evans aggregation index (Clark and Evans, 1954). The clustering index (CI) was calculated as the ratio between average observed and expected (i.e., for random point patterns) nearest-neighbor distance. CI increases from fully clustered (CI = 0 if the distance between nearest neighbors is equal to the minimal distance for all neurons) to random (CI = 1) to grid-like distributions of neurons (CI > 1, depending on the cell density). Note that CI is insensitive to a potentially grid-like arrangement of clusters (i.e., the next level of structural organization), which we do not analyze in this study. Under realistic circumstances, the distances between neurons must be a least the diameter of cell bodies, which leads to longer average nearest-neighbor distances and an underestimation of clustering. To account for this, we simulated random distributions with equal density using the average cell body diameter (10 μm) as minimal possible distance by successively adding neurons to randomly drawn positions and rejecting neurons that would overlap with others (Galli-Resta et al., 1999). We further extended the

analysis to assess cluster sizes by calculating the n^{th} nearest-neighbor distances in networks and simulated random distributions.

Neurite morphology was examined by immunocytochemical staining of microtubule-associated protein 2 (MAP2; chicken-anti-MAP2; 1:500; Abcam) and phosphorylated neurofilament 200 kDa (rabbit-anti-neurofilament; 1:10; Abcam) to visualize dendritic and axonal compartments, respectively. To detect axons and dendrites, images for the respective channels were high-pass filtered. In a second step, a peak detection was performed for each row of the resulting image (peaks corresponded to neurites; detection resolution of 2 μm intervals between intersections). To avoid a bias due to strongly orientated neurites, the procedure was repeated for different orientations (in steps of 30°; implemented by image rotation). Neurite counts and intervals of all scans were pooled. Axodendritic intersections were marked at the center-of-mass of patches of colocalized axon-positive and dendrite-positive pixels (at any angle), allowing deviation of 1 pixel width (0.645 μm). To determine the degree of neurite fasciculation, we took the mean interneurite intervals divided by the SD as fasciculation index (FI). This provided a measure similar to the CI for the cell body distribution: FI increases from fully fasciculated (FI = 0; minimal distance between neurites) to random (FI = 1) to grid-like neurite arrangements (FI > 1).

Dendritic morphology was examined in sparse networks by Sholl analysis (Sholl, 1953). All morphological analyses were made with Matlab. Significance is specified by p values determined with the Student's t test (p_{stt}) for independent samples.

Patch-clamp recording and analysis. Patch pipettes [6.3 ± 1.4 MΩ (mean and SEM)] were filled with a intracellular solution containing the following: potassium D-gluconate (125 mM; Sigma-Aldrich), KCl (20 mM; Sigma-Aldrich), EGTA (5 mM; Carl Roth), Na_2-ATP (2 mM; Carl Roth), HEPES (10 mM; Carl Roth), $MgCl_2$ (2 mM; Sigma-Aldrich), $CaCl_2$ (0.5 mM; Sigma-Aldrich), and biocytin (10 mg/ml, Invitrogen), adjusted with KOH to pH 7.4, and with sucrose to 320 mOsm. Patch-clamp recordings in whole-cell configuration were conducted at 37°C (PH01 perfusion heating, Multi Channel Systems; TC02 temperature controller, Multi Channel Systems) and perfusion with carbogenated (95% O_2 and 5% CO_2; Air Liquide) culture medium without horse serum and without Gö6976 and PMA. Data were sampled at 25 kHz (Micro1401 amplifier and Spike2 software; Cambridge Electronics Design). Up to four neurons were recorded per network for ~30 min each. Input resistances were determined with hyperpolarizing current pulses (−50 pA). Datasets of ≥20 min were analyzed with Matlab. The SD of V_m was averaged for time bins of 1 s. The first step to detect EPSPs was to bootstrap an EPSP template from the data. Putative events were detected with a threshold set manually for V_m slope. Snippets surrounding detection time points t_D were classified by hierarchical clustering and the EPSP template was subsequently derived as the average of a manually chosen cluster resembling the voltage time course of typical isolated EPSPs. Based on this template, EPSPs were detected by correlation of V_m with the onset phase of the template (−5 to 10 ms around t_D) and a correlation threshold of 0.5.

Extracellular recording and analyses. Multiunit spike activity was recorded from microelectrode arrays (MEAs; MEA1060-BC, USB-MEA256-System, and MEA 30-1024-System amplifiers; Multi Channel Systems, 25 kHz sampling frequency, 12 bit) under culture conditions (37°C, 5% CO_2) and acquired with MCRack software (Multi Channel Systems; versions 3.3–4.0). Recordings of individual networks lasted ≥1 h. Action potentials (APs) were detected with a threshold set to −5 SDs of the high-pass-filtered baseline signal (Butterworth second-order high-pass filter, 200 Hz cutoff; detection dead time, 2 ms). Stimulation was controlled using a programmable stimulus generator (STG2004, Multi Channel Systems). A single stimulus consisted of a monophasic negative pulse with 400 μs width and 0.6 V amplitude. Stimulation electrode sequences were controlled by MEABench (version 1.0.16; Wagenaar and Potter, 2004). After a baseline recording period of ≥30 min of spontaneous activity, all array electrodes were stimulated consecutively at interstimulus intervals of either 6, 4, or 2 s. The sequence was repeated 20 times in succession.

Raw data from MEA recordings were imported into Matlab using MEA-Tools (Egert et al., 2002) and the Find toolbox (Meier et al., 2008). Spontaneous SBEs were detected as follows: series of spikes with consecutive interspike intervals shorter than a threshold value (100 ms) were detected as bursts. SBEs were defined as periods in which a predefined fraction of electrodes showed simultaneous bursts (10% of active sites, minimally 3, maximally 20 to keep criteria comparable between small and large MEAs). To account for buildup and fading phases of SBEs, spikes within a time windows of 25 ms before and following this SBE core were included into the SBE. Network activity was characterized by the following parameters: the rate of SBEs in the recording period, burst strength as the average number of APs per SBE and active site, average firing rate (AFR) as the gross average firing rate across all active sites, and SBE recruitment as the average fraction of active sites participating in SBEs. For experiments with PTX, we defined as control period the last 1 h section before application of PTX and excluded the first 10 min after application from the analysis to avoid transients. In stimulation experiments, we excluded the first 10 ms after stimuli to blank stimulation artifacts.

Propagation pattern analysis. To analyze spatiotemporal propagation patterns, SBEs were classified by first-spike rank order, i.e., electrodes were ranked by the relative timing of the first spike recorded at a given electrode during SBEs. Similarity between SBEs was calculated as the Spearman correlation of the resulting electrode sequences. Groups of similar patterns were identified by correlation-matrix-based hierarchical clustering (complete linkage) using one minus the correlation value as the distance measure (Liu et al., 2012). Distances <1 indicate correlated patterns. Distances >1 indicate anticorrelated patterns. To assess the richness of patterns, we determined the number of classes yielded at a given distance threshold between 0.02 and 2. As the contribution of individual classes, we calculated the cumulative fraction of SBEs accounted for by the most frequent pattern classes for series of 100 SBEs.

SBE initiation zones. BIZs were identified in recordings from large MEAs (16 × 16 and 32 × 32 electrode grid layouts) that spanned almost the entire network area. On these arrays, the median x and y coordinates of the first 10 active sites that fired during SBEs were used to localize the spatial SBE onset position. Note that this approach produced a slight bias of BIZs toward the array center. The spatiotemporal structure of SBE initiation process was further analyzed as firing rate relative to SBE onset time (2 ms bins) and distance to respective BIZs (300 μm bins, i.e., electrode pitch) averaged across 500 consecutive SBEs.

Results

PKC promotes cell migration and clustering of neuronal cell bodies

Neuronal networks were prepared from neonatal rat cortex with ~600–800 neurons/mm^2 surviving at 20 DIV. This variability is unlikely to be relevant for the overall level of network activity (Biffi et al., 2013). Following intense neurite outgrowth, these networks developed spontaneous activity with SBEs as early as 5 DIV.

Under PKC^N conditions (i.e., with normal PKC activity), neuronal somata migrated and aggregated, establishing a soma density landscape with high-density clusters within 3 weeks (Fig. 1*A*). To find the minimal distance between neurons, we calculated the Euclidean distance distribution for the edges derived from a Delaunay triangulation of neuron positions. In all pharmacological conditions, we found a minimal distance of ~10 μm between cell body centers, which corresponds to their soma diameter (Fig. 1*B*). The degree of clustering after development was quantified following the Clark–Evans aggregation index (Clark and Evans, 1954), i.e., the ratio of the observed mean nearest-neighbor distance in the network to that expected for a Poisson point process with the same spatial density, modified to take into account the minimal possible distance of 10 μm between soma centers (Fig. 1*C*). A CI of <1 denotes clustering and a CI >1 denotes dispersion of neuronal somata relative to the expectation. PKC^N networks were strongly clustered at 20 DIV compared with almost random spatial distributions in networks

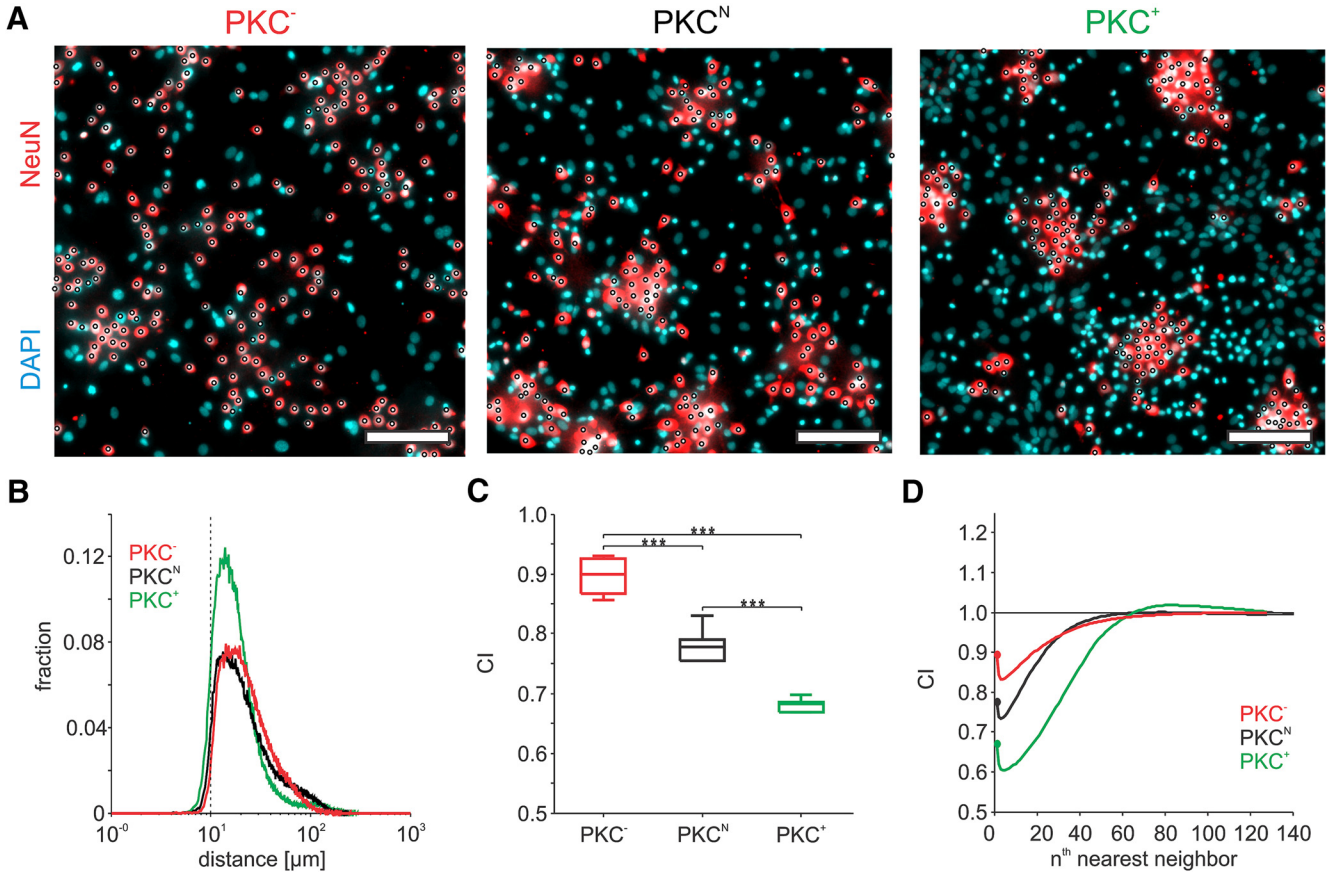

Figure 1. Generic network structure and activity dynamics in networks of cultured cortical neurons. ***A***, Staining of neuronal nuclei (NeuN; red) and all cellular nuclei (DAPI; blue) in networks at 20 DIV that had developed under inhibited (PKC^-), normal (PKC^N), and enhanced PKC (PKC^+) activity. Neurons were detected (white circles) and analyzed for their spatial distributions. Scale bars, 100 μm. ***B***, Distributions of minimal distances between soma centers of pairs of neighboring neurons. Distances were $\geq$10 μm, indicating that the soma diameter was ~10 μm (dashed line). ***C***, Clark–Evans CI for nearest-neighbor distances indicates significantly weaker clustering in PKC^- and stronger clustering in PKC^+ networks compared with PKC^N networks. ***D***, CIs <1 up to the n^{th} nearest neighbor indicate typical cluster sizes in the range of $\leq$60 neurons. Boxplots show median, 25th, and 75th percentiles and minimal and maximal values (excluding outliers). ***$p_{stt} = 0.001$.

shortly after seeding at 1 DIV (CI mean ± SEM: 20 DIV, 0.78 ± 0.03; 1 DIV, 1.0 ± 0.02; $n = 6$, $p_{stt} = 1.3*10^{-12}$). We further calculated the cluster index for the n^{th} nearest neighbors to assess the average number of neurons in clusters. At 20 DIV, CI for the n^{th} nearest neighbors (CI_n) was significantly reduced approximately up to the 45th nearest neighbor ($p_{stt} < 0.01$, pairwise testing), indicating typical cluster sizes in this range (Fig. 1*D*).

To modify the degree of clustering and to investigate its relevance for the spatiotemporal structure of activity in these networks, we increased respectively inhibited PKC activity during network development. Increasing PKC activity by PMA (1 μM; PKC^+) during network development promoted neuronal aggregation compared with PKC^N networks (CI, 0.67 ± 0.02; $n = 5$, $p_{stt} = 1.1*10^{-4}$) and resulted in networks with strikingly regularly spaced, well delineated clusters at 20 DIV (Fig. 1*A*). Although clustering was increased in PKC^+ networks (Fig. 1*C*), typical cluster sizes were only slightly larger than in PKC^N networks, with CI_n significantly reduced for the first 50 nearest neighbors ($p_{stt} < 0.01$ for pairwise testing; Fig. 1*D*). In contrast, chronic PKC inhibition by Gö6976 diminished cell migration and led to more homogeneously distributed neuronal somata (Fig. 1*A*) with a significantly lower degree of clustering (CI, 0.90 ± 0.04; $n = 5$; $p_{stt} = 3.6*10^{-4}$; Fig. 1*C*) compared with PKC^N networks and PKC^+ networks. Remaining cell aggregation resulted in areas with slightly increased density but with weak contrast to the background density of neurons. Again, these denser areas contained ~50 neurons (Fig. 1*D*).

PKC promotes fasciculation and local density of neurites

Substantial neurite outgrowth started within hours after seeding. We quantified the density and arrangement of neurites in mature networks at 20 DIV based on immunohistochemical staining for MAP2 in dendrites and neurofilament in axons (Fig. 2*A*). Neurite densities were determined by counting neurite intersections with straight lines drawn across the network (Fig. 2*B*,*C*).

PKC^N networks had high dendrite densities (125.3 ± 9.3 dendrites/mm, mean ± SEM, $n = 6$; Fig. 3*A*) with relatively homogeneous coverage (FI, 0.84 ± 0.01; Fig. 3*B*). The density of axons (61 ± 8 axons/mm; Fig. 3*C*) was lower than that of dendrites, and axons also formed bundles between clusters (FI, 0.73 ± 0.09, mean ± SEM; Fig. 3*D*). Note that this does not mean that axons connected exactly two adjacent clusters. Some axons spanned distances of several millimeters and could pass through several clusters.

Following the clustering of somata, increasing PKC activity had a profound impact on the arrangement of neurites. The overall density of dendrites decreased in PKC^+ networks (99 ± 9 dendrites/mm, $p_{stt} = 9.8*10^{-4}$, $n = 5$ networks). Furthermore, dendrites were densely aggregated in neuron clusters, leaving regions with lower dendrite density in between clusters (Fig. 2*B*). Fasciculation of dendrites was significantly increased in PKC^+ networks (FI, 0.78 ± 0.04; $p_{stt} = 2.7*10^{-4}$). The density of axons likewise was significantly reduced compared with PKC^N networks (49 ± 5 axons/mm, $p_{stt} = 3.3*10^{-2}$, $n = 5$). As in PKC^N networks, axons fasciculated and formed bundles between soma

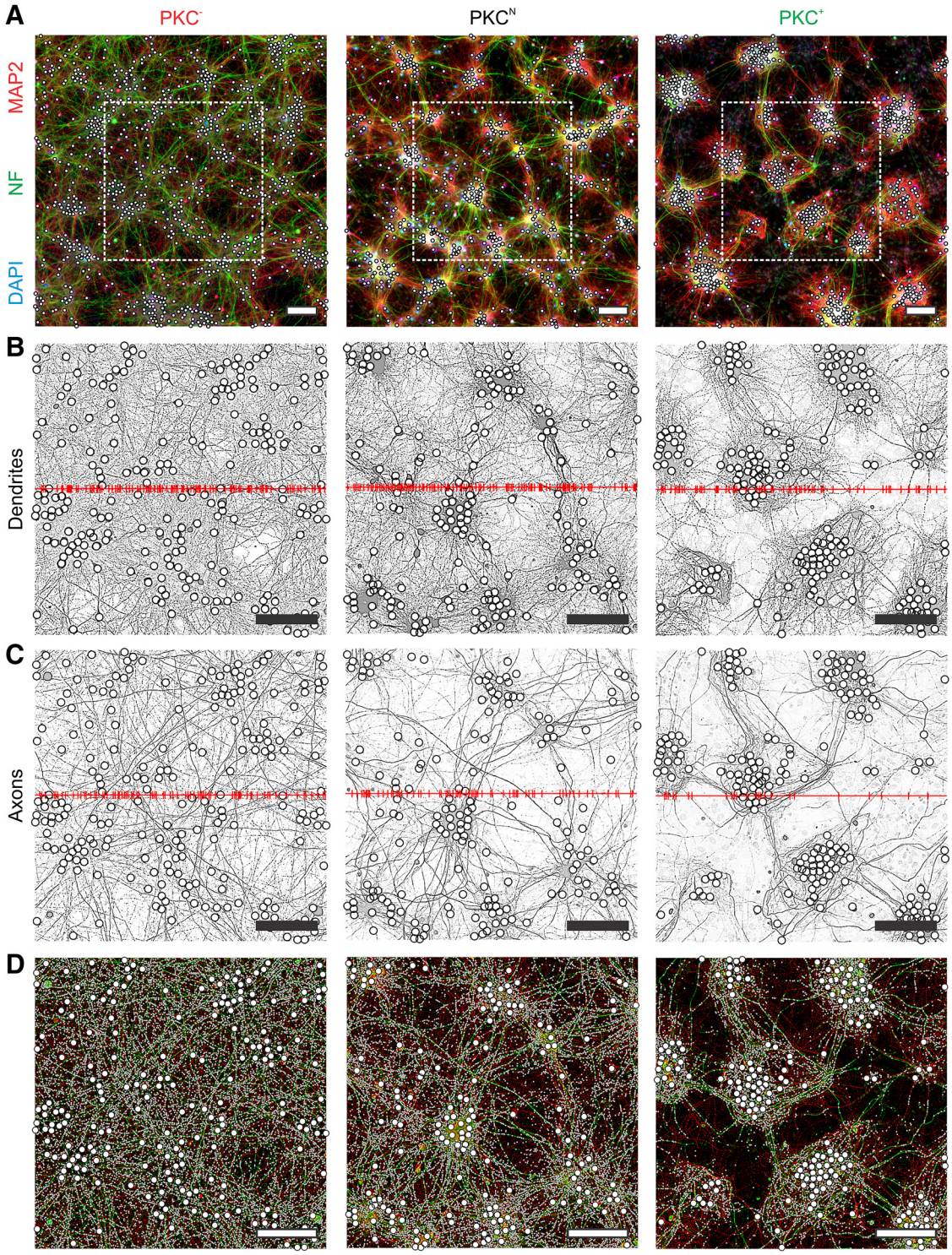

Figure 2. Manipulating PKC activity changes the mesoscopic network architecture. ***A***, Staining of axons (anti-neurofilament; green) and dendrites/cell bodies (anti-MAP2; red) and NeuN (blue). The dashed square indicates the panel positions in Figure 1*A* and white circles indicate the detected neuronal somata. Under PKC^N conditions, axons and dendrites fasciculated and cell bodies clustered. PKC inhibition resulted in more homogeneous axon and dendrite coverage, and soma distributions. Enhanced PKC activity resulted in well delineated clusters with strongly entangled dendrites and axons that interconnected clusters in bundles and looped within clusters. ***B***, ***C***, To quantify fasciculation and density, dendrites (***B***) and axons (***C***) were analyzed in high-pass filtered images of red and green channels, respectively, by detecting intensity peaks in image rows. Neurite detections for one row are shown in red. The FI was calculated based on the distribution of intervals between peaks. Note that neurite densities decrease from PKC^- over PKC^N to PKC^+. ***D***, Intersections (small white dots) of axons and dendrites provide a lower bound estimate for putative synaptic sites. The spatial distribution of intersections was concordant to the distributed or clustered arrangement of cell bodies (large circles) and neurites. Scale bars, 100 μm.

clusters (FI, 0.69 ± 0.05). Within clusters, axons strongly ramified and formed local loops.

In contrast to chronic PKC stimulation, developmental PKC inhibition significantly increased dendrite and axon densities (141 ± 3 dendrites/mm, $p_{stt} = 1.2*10^{-2}$; 131 ± 7 axons/mm, $p_{stt} = 6.5*10^{-7}$, $n = 4$) compared with PKC^N networks.

To validate the effect at the single-neuron level, we further analyzed the extent of dendritic fields by Sholl analysis in sparse cultures

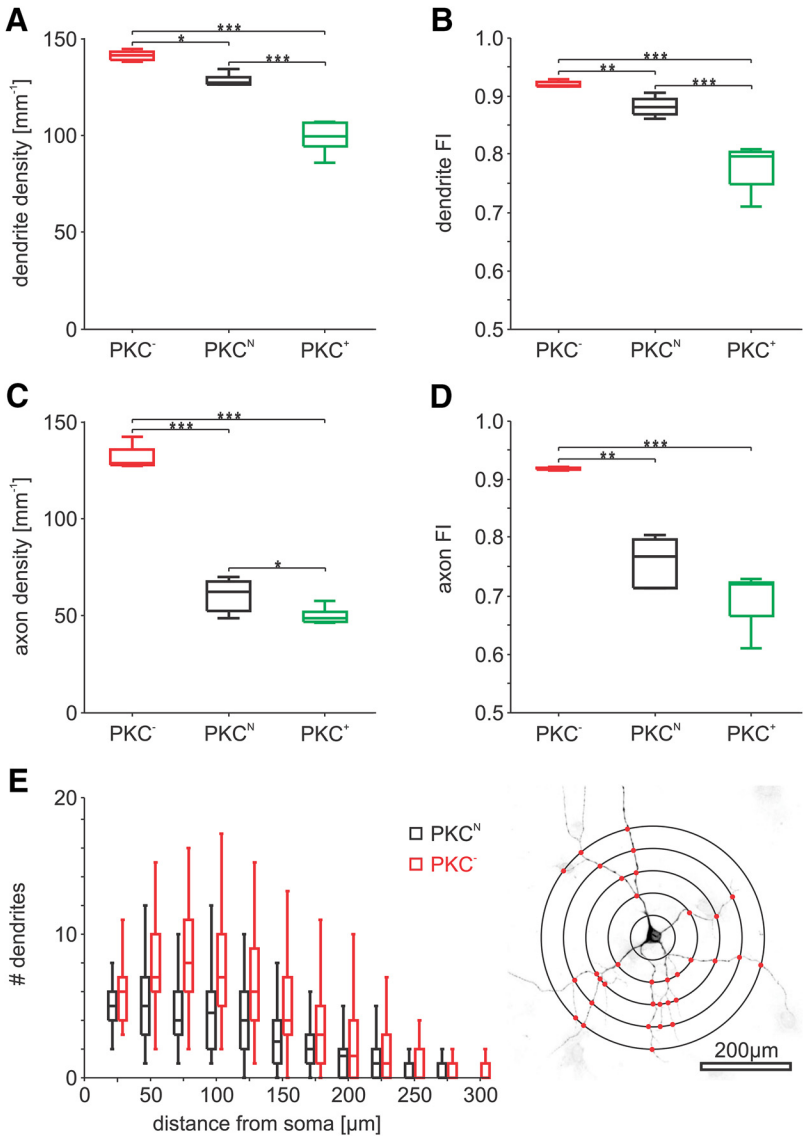

Figure 3. Distribution and density of neurites in different PKC activity conditions. ***A***, Dendrite densities in networks decreased significantly with increasing PKC activity. ***B***, Neurite fasciculation increased with PKC activity. ***C***, ***D***, Changes of PKC activity levels had the same and even stronger effects on axons. ***E***, Dendrites were analyzed by Sholl analysis in sparse cultures stained with antibodies against MAP2 at 24 DIV. PKC inhibition increased the average number of dendritic branches at any distance from the soma, thereby producing larger dendrites. Boxplots show median, 25 th, and 75 th percentiles and minimal and maximal values (excluding outliers). *$p_{stt} = 0.05$; **$p_{stt} = 0.01$; ***$p_{stt} = 0.001$.

at 24 DIV (Fig. 3*E*). Chronic PKC inhibition increased dendrite branching and extent, resulting in significantly increased total dendrite length (PKC^N, 1449 ± 647 µm; $N = 58$ neurons; PKC$^-$, 2132 ± 816 µm; $N = 78$ neurons; $p_{stt} = 5.6*10^{-7}$). In addition to increasing neurite densities, PKC inhibition significantly diminished dendritic (FI, 0.92 ± 0.01, $p_{stt} = 2.5*10^{-3}$) and axonal (FI, 0.92 ± 0.002, $p_{stt} = 4.2*10^{-3}$) fasciculation, leading to a much more homogeneous neurite coverage than in PKC^N networks.

Synaptic connectivity

As a lower estimate of the number of potential synapse sites in different network types, we detected intersections between axons and dendrites (Fig. 2*D*). PKC^N networks yielded ~40,000 intersections/mm^2, corresponding to ~100 sites per neuron. Note that due to the limited spatial resolution of the analysis, in particular in clusters and neurite bundles, this number considerably underestimated the real density of synapses but enabled estimates over large areas of the network. The more homogeneous arrangement of neurites in PKC$^-$ networks entailed a corresponding distribution of axodendritic intersections. In PKC$^-$ networks, we determined the highest number of axodendritic intersections of ~70,000 sites/mm^2, much higher than in PKC^N networks and consistent with the high neurite density. In contrast, the overall density in PKC$^+$ networks of ~30,000 sites/mm^2 was slightly lower than in PKC^N networks. As a consequence of the local tangles of neurites, axodendritic intersections were spatially clustered in PKC$^+$ networks.

Changes in the distribution of axodendritic contact sites likely influence the connectivity of the network and thus the synaptic input to individual neurons. Such changes could be critical for the initiation and propagation of spontaneous network activity. We thus analyzed synaptic dynamics in whole-cell patch-clamp recordings during spontaneous network activity between 18 and 30 DIV for neurons grown in different PKC activity conditions (number of neurons and networks: PKC^N $n = 45$ neurons, 16 networks; PKC$^-$ $n = 45$ neurons, 21 networks; PKC$^+$ $n = 20$ neurons, 10 networks).

Neurons in PKC$^-$ and PKC^N networks had comparable input resistances (PKC^N, 233 ± 14 MΩ, mean ± SEM; PKC$^-$, 225 ± 16 MΩ). In PKC$^+$ networks, however, input resistances were significantly lower (PKC$^+$, 136 ± 19 MΩ; $p_{stt} = 6.5*10^{-4}$ vs PKC^N). Resting potentials varied across neurons and were significantly more negative in PKC$^-$ networks (PKC$^+$, −50.4 ± 1.7 mV, mean ± SEM; $p_{stt} = 0.08$ vs PKC^N; PKC^N, −53.8 ± 1.0 mV; PKC$^-$, −57.6 ± 1.2 mV, $p_{stt} = 0.02$ vs PKC^N). Average thresholds of AP initiation did not differ significantly between network types (PKC^N, −42.5 ± 0.7 mV; PKC$^-$, −41.9 ± 1.4 mV; PKC$^+$, −39.3 ± 2.0 mV). To measure EPSP activity under comparable conditions, the resting potential of all neurons was set to ~−65 mV by constant current injection.

In all networks, V_m fluctuated around the resting V_m between SBEs and underwent strong depolarization for several hundred milliseconds, during which APs were generated (Fig. 4*A*). These up states corresponded to SBEs measured extracellularly (Fig. 5*A–C*). V_m fluctuation between SBEs increased from PKC$^-$ to PKC^N to PKC$^+$ networks (SD of V_m: PKC$^-$, 0.95 ± 0.12 mV; PKC^N, 1.97 ± 0.13 mV; $p_{stt} = 8.2*10^{-8}$; PKC$^+$, 2.25 ± 0.43 mV).

To further determine how the embedding of individual neurons into the network affected V_m variability, we classified neurons according to their membership in clusters. This revealed that V_m of neurons within clusters fluctuated more than that of

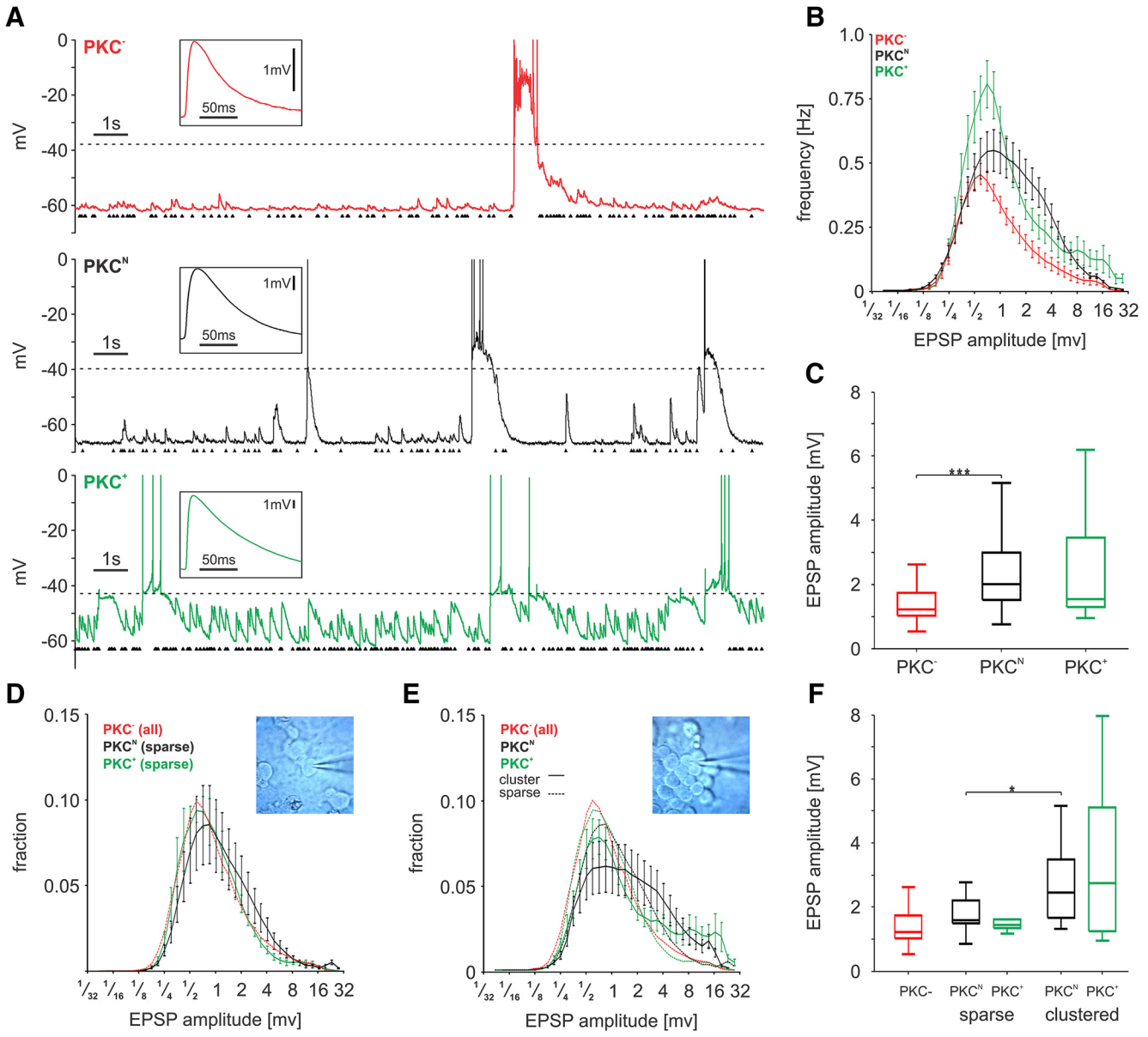

Figure 4. Intracellular recordings from neurons in different mesoscopic network architectures. ***A***, V_m traces from neurons recorded in PKC$^-$, PKC^N, and PKC$^+$ networks at 20 DIV display EPSP activity (black arrows) and strong depolarizations corresponding to SBEs. The AP threshold ~ -40 mV is indicated by the dashed line. Insets, Average shape of nonoverlapping EPSPs in between SBEs. ***B***, ***C***, Average amplitude distributions across neurons reveal a larger fraction of smaller EPSPs in PKC$^-$ networks than in PKC^N networks. Strongly clustered PKC$^+$ networks had a bimodal amplitude distribution with smaller and large EPSPs. ***D***, Neurons were classified according to their local neuronal neighborhood. EPSP amplitude distributions for neurons in sparse regions did not differ significantly between conditions. ***E***, ***F***, Clustered neurons in PKC^N and PKC$^+$ networks had larger EPSP amplitudes than neurons in sparse regions. Boxplots show median, 25th, and 75th percentiles and minimal and maximal values (excluding outliers). *$p_{stt} = 0.05$; ***$p_{stt} = 0.001$.

neurons in sparse regions in PKC^N networks (SD of V_m: sparse, 1.60 ± 0.14 mV; $n = 14$; cluster, 2.44 ± 0.27 mV; $n = 16$; $p_{stt} = 5.9*10^{-3}$) and PKC$^+$ networks (sparse, 1.19 ± 0.18 mV; $n = 6$; cluster, 2.87 ± 0.60 mV; $n = 13$). PKC$^-$ networks had no clear clusters to assess such dependence.

As a potential source of these differences, we assessed the effective strength of synaptic inputs in different network types by analyzing identifiable EPSPs during interburst periods. In PKC^N networks, EPSPs occurred at 8.1 ± 0.6 Hz (mean ± SEM). EPSPs amplitudes were approximately lognormally distributed (2.3 ± 0.2 mV; Fig. 4*B*,*C*). Occasional fast subthreshold excursions of V_m >10 mV possibly corresponded to multisynaptic input from the same neuron. In PKC$^-$ networks, EPSPs rates in between SBEs were significantly lower (5.0 ± 0.5 Hz, $p_{stt} = 7.8*10^{-5}$) with much lower EPSP amplitudes (1.5 ± 0.1 mV, $p_{stt} = 6.1*10^{-4}$). In contrast, in the strongly clustered PKC$^+$ networks, EPSPs rates were 9.1 ± 0.6 Hz ($p_{stt} = 3.7*10^{-6}$ vs PKC$^-$) with an average amplitude of 2.7 ± 0.5 mV ($p_{stt} = 2.2*10^{-3}$ vs PKC$^-$ networks).

Since synaptic properties could depend on the local embedding of neurons into the network, we again classified neurons according to their position within or outside a cluster. In neurons outside of clusters, EPSP amplitude distributions and the average EPSP amplitudes were similar in all network types (PKC^N, 1.8 ± 0.2 mV; PKC$^-$, 1.5 ± 0.1 mV; PKC$^+$, 1.5 ± 0.1 mV; Fig. 4*D*,*F*). Neurons located within clusters, however, had higher average EPSP amplitudes (PKC^N, 2.8 ± 0.4 mV; $p_{stt} = 0.02$; PKC$^+$, 3.3 ± 0.6 mV; Fig. 4*E*,*F*), whereas EPSP

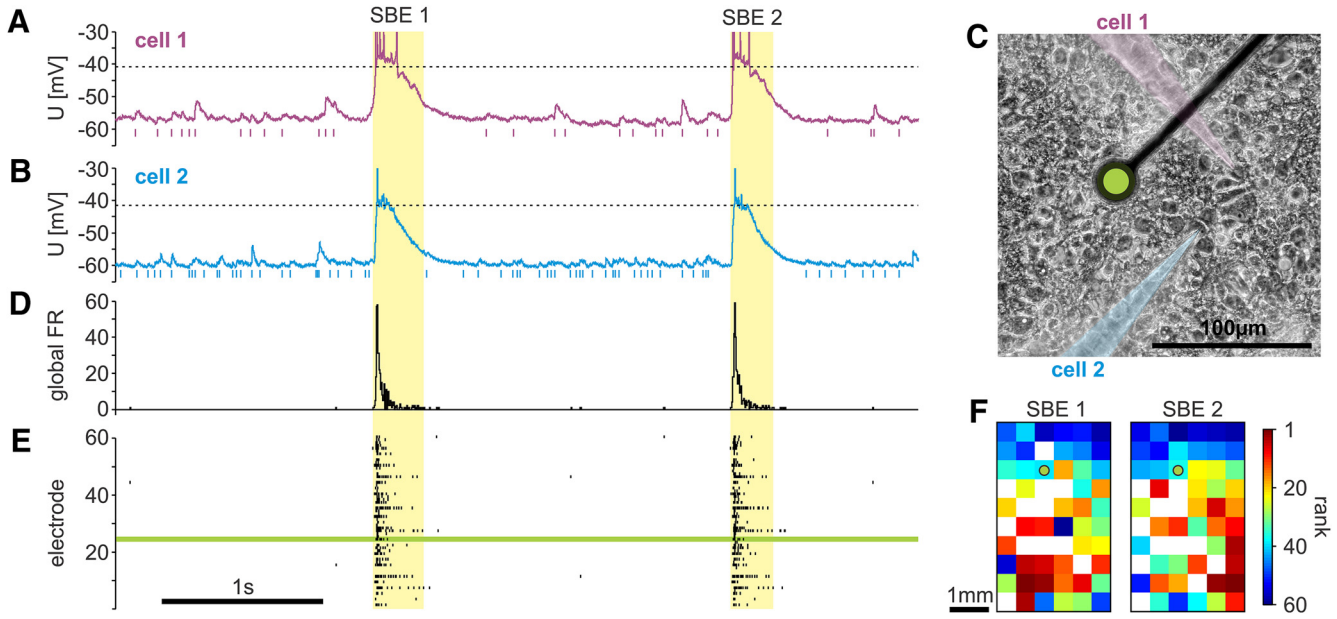

Figure 5. Paired intracellular and MEA recordings. ***A***, ***B***, V_m traces from two neurons near an MEA electrode. ***C***, EPSPs are indicated by vertical ticks beneath the traces and the dashed horizontal line indicates the spiking threshold at ~ −40 mV. Baseline EPSP activity is interrupted by V_m up states, during which these neurons generated spikes. ***D***, ***E***, V_m up states coincide with network-wide SBEs recorded with the MEA. ***F***, Propagation patterns were defined from the order of the first spikes at each electrode after detection of SBE onset, shown here for these two consecutive SBEs. Green line in ***E*** indicates MEA electrode marked in ***C***.

rates in clustered and nonclustered neurons did not differ significantly.

Clustering promotes spontaneous bursting activity

V_m dynamics in individual neurons reflect the ongoing AP dynamics in recurrent networks subsampled by their particular afferent population. To assess the spontaneous network-wide dynamics, we recorded extracellular spike activity over extended time periods with MEAs. SBEs corresponded to up states measured intracellularly (Fig. 5*A–C*) and represented the dominating spontaneous activity pattern, clearly standing out from the uncorrelated background activity in all network types. At onset, SBEs typically propagated across the network with a traveling wave front (Fig. 5*F*). In all networks, typically >80% of spikes were part of SBEs (Fig. 6*A*; recording at 25–35 DIV; PKC^N, 95 ± 1%; $n = 22$; PKC^-, 85 ± 3%, $n = 18$; PKC^+, 97 ± 1%, $n = 7$). Consistent with the higher rate of V_m up states observed intracellularly, the frequency of SBEs increased with the degree of clustering in networks (Fig. 6*B*).

SBE rates increased from PKC^- networks (2.0 ± 0.3 SBE/min; $p_{stt} = 1.4*10^{-8}$ vs PKC^N) and PKC^N networks (13.0 ± 1.4 SBE/min) to PKC^+ networks (29.5 ± 5.0 SBE/min, $p_{stt} = 1.8*10^{-4}$ vs PKC^N).

Furthermore, the temporal variability of SBE initiation significantly increased with the degree of clustering in networks (Fig. 6*F*). In some networks, SBE rates fluctuated strongly, with periods of strongly increased bursting comparable to superbursts described by Wagenaar et al. (2006a). These superbursts occurred in almost all PKC^+ networks, occasionally in the moderately clustered PKC^N networks, and rarely in the PKC^- networks.

SBEs typically did not involve the entire network. The fraction of the network recruited in individual SBEs decreased with the degree of clustering (Fig. 6*E*). In PKC^- networks, a significantly higher fraction of all active sites participated in individual SBEs, compared with the clustered PKC^N and PKC^+ networks (PKC^N, 67 ± 4%; PKC^-, 86 ± 3%; $p_{stt} = 1.8*10^{-3}$; PKC^+, 54 ± 5%; $p_{stt} = 1.8*10^{-3}$ vs PKC^-).

Gross AFRs (Fig. 6*D*) across recording sessions of ≥1 h were significantly lower in PKC^- networks (0.35 ± 0.05 Hz, $p_{stt} = 6.6*10^{-4}$) compared with PKC^N networks (1.50 ± 0.28 Hz). Despite their much higher SBE rate, AFRs in PKC^+ networks (1.49 ± 0.15 Hz) were not significantly higher than in PKC^N networks. This was due to an inverse correlation between SBE rate and burst strength, i.e., the average number of spikes per SBE and site. In consequence, high SBE rates entailed weaker bursts (PKC^-, 10.9 ± 1.9 spikes/site; PKC^N, 7.8 ± 1.3 spikes/site; PKC^+, 3.5 ± 0.7 spikes/site; $p_{stt} = 0.026$ vs PKC^-; Fig. 6*B*). The bursting strength was more variable in clustered networks where individual sites displayed varying numbers of spikes during SBEs (Fig. 6*G*).

Network metastructure influences the richness of activity patterns

The higher SBE variability in terms of burst size, network recruitment, SBE intervals, and the occurrence of superbursts in PKC^N and PKC^+ networks suggests that clustering promoted the richness of activity, which in this context refers to the spectrum of temporal and spatial patterns of spike activity and their pathways of propagation within a network. Based on MEA recordings, we identified SBE propagation patterns as the rank order of burst onset at individual electrodes (delay of first spike after SBE onset). Such order-based representation of SBE activity, compared with temporal representations that preserve exact delays, was demonstrated to be more robust for reconstructing SBE origins and less dependent on detecting the true first spike of a pattern (Shahaf et al., 2008).

SBEs typically spread with a traveling wave front, which was irregular in PKC^N networks, but smooth and regular in the more homogeneous PKC^- networks as well as in the strongly clustered PKC^+ networks. Propagation pattern similarity was determined as the Spearman correlation of first-spike rank-order sequences

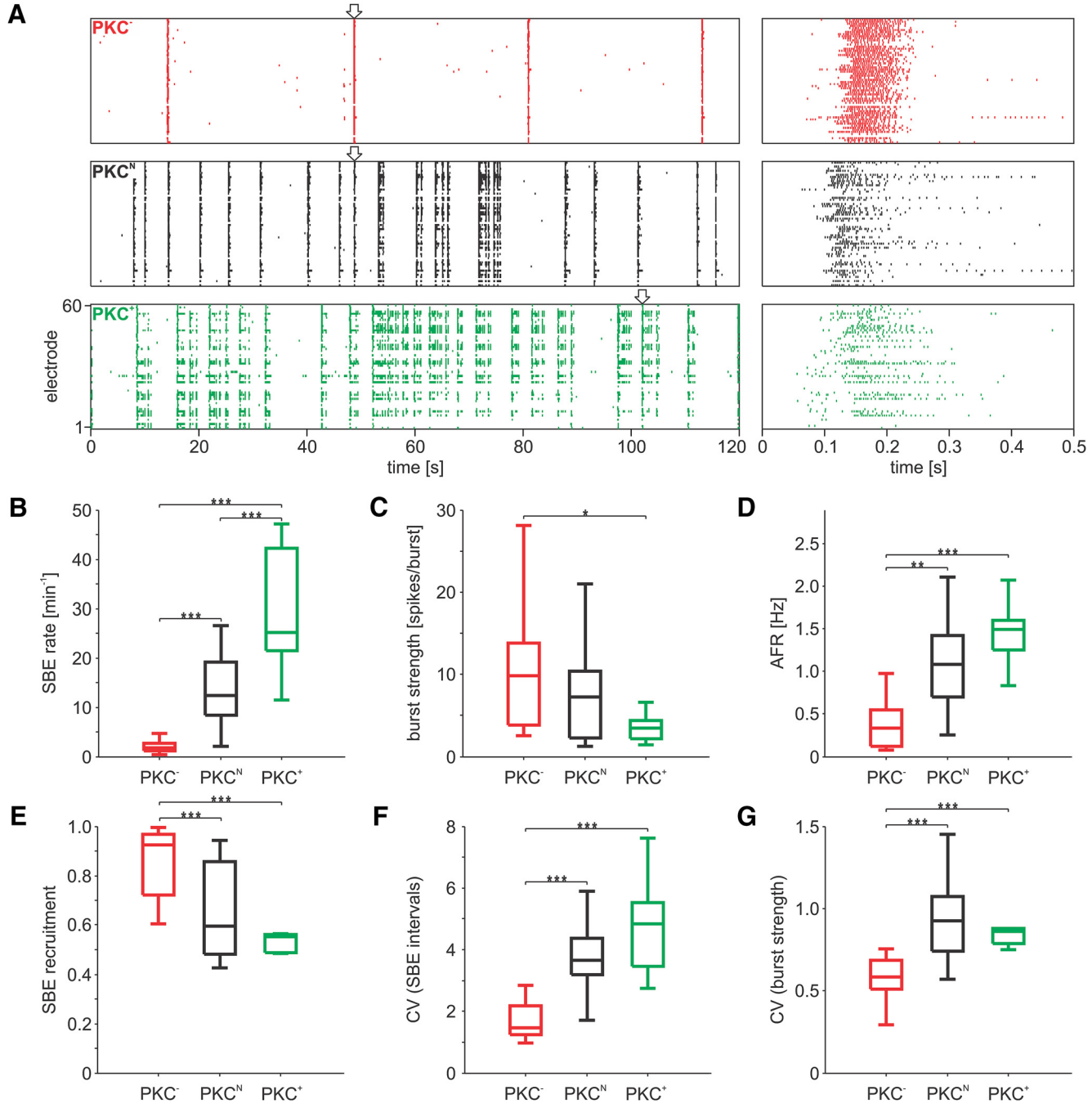

Figure 6. Spontaneous SBE activity at 30 DIV in networks recorded with MEAs. ***A***, In all network architectures, spontaneous network activity consisted of SBEs and low levels of spiking in between. Right, Zoom into SBEs marked by the arrow on the left. The spatiotemporal structure of SBE activity differed remarkably in networks with different structures. Spontaneous SBE rates, gross activity levels, and spatiotemporal variability increased with the degree of clustering in networks from PKC^{-} to PKC^{+} networks. The strength of neuronal recruitment during SBEs and the bursting strength decreased along this axis. ***B***, Spontaneous SBE rates. ***C***, Bursting strength, i.e., the mean number of APs per site and SBE. ***D***, AFRs, i.e., the average AP frequency across all site with activity in the 1 h recording session. ***E***, SBE recruitment, i.e., the average fraction of active sites recruited during SBEs. ***F***, The irregularity of SBE initiation given as the coefficient of variance (CV) of inter-SBE intervals. ***G***, Variability in the intensity of neuronal firing during SBEs as average CV of bursts strengths (#APs/SBE) determined for individual sites. Boxplots show median, 25th, and 75th percentiles and minimal and maximal values (excluding outliers). $^{*}p_{stt} = 0.05$; $^{**}p_{stt} = 0.01$; $^{***}p_{stt} = 0.001$.

across SBEs (Fig. 7*A*). In PKC^{N} networks, correlation-matrix-based hierarchical clustering (Liu et al., 2012) did not reveal conspicuous pattern classes. In contrast, PKC^{-} as well as PKC^{+} networks showed clear clusters of highly similar propagation patterns (Fig. 7*A–C*) with a high intraclass correlation and low or negative (distances >1) interclass correlation.

To compare the diversity of these propagation patterns across networks, we determined the number of classes with patterns correlated above a given threshold (Fig. 7*D*). Intermediate distance thresholds between 0.02 and 0.8 (correlation coefficient, 0.2–0.98), yielded significantly fewer classes in PKC^{-} networks than in PKC^{N} networks ($p < 0.01$), indicating that SBE propagation patterns clustered in few groups with high intragroup similarity in PKC^{-} networks. While this might suggest that diversity increases with clustering, the more strongly clustered network structure found in PKC^{+} networks did not further promote the

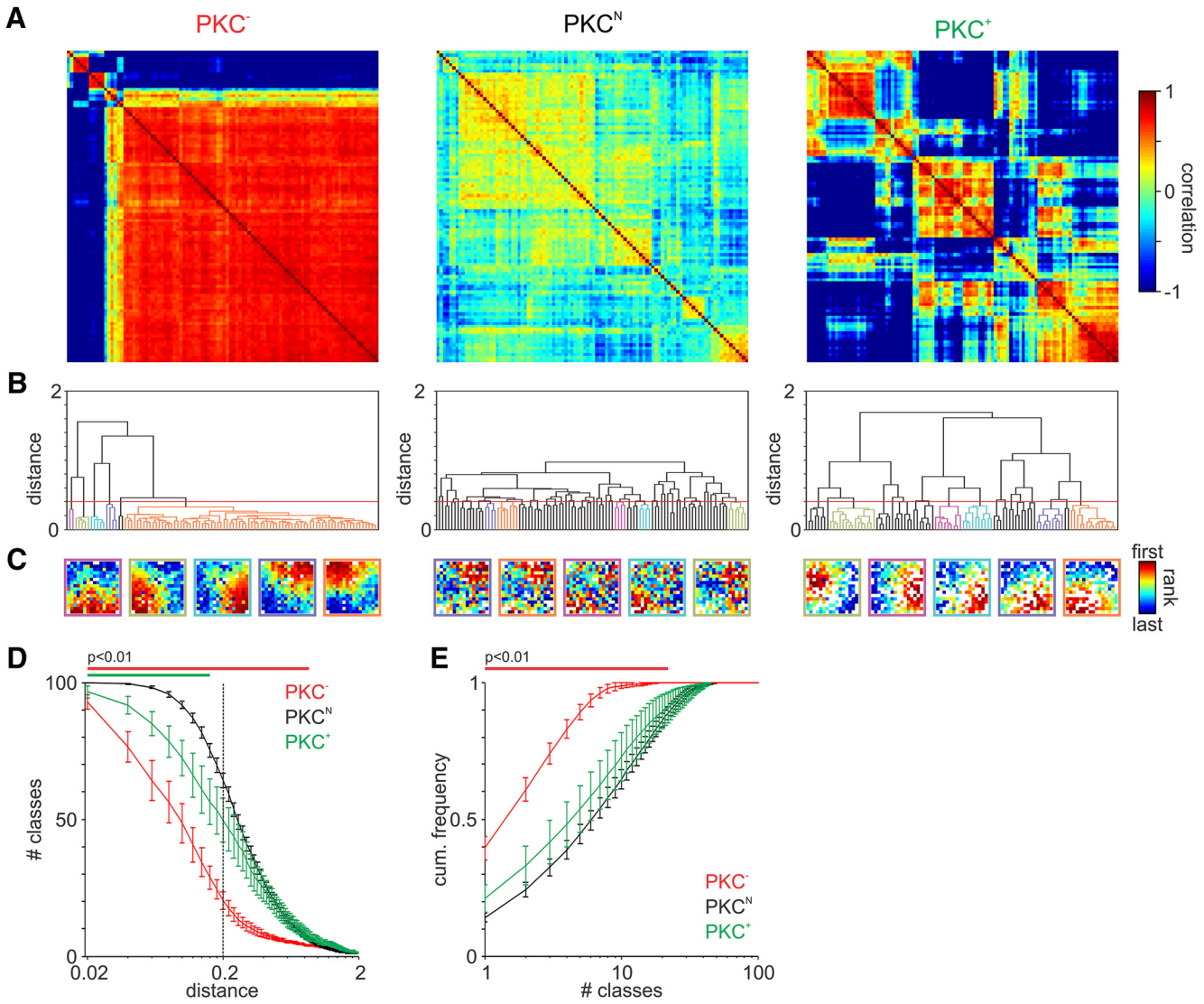

Figure 7. Diversity in SBE propagation patterns. ***A***, Spearman correlation matrices for first-spike rank-order sequences in SBEs ($N = 100$ SBEs, 1 network per condition). ***B***, Corresponding dendrograms for complete linkage clustering. PKC^- networks typically displayed a few distinct propagation pattern classes, while PKC^N networks were marked by a continuum of gradually differing patterns. Strongly clustered PKC^+ networks had many distinct pattern classes. ***C***, Average propagation patterns for classes for a threshold distance of 0.2 (corresponding to a Spearman correlation coefficient of 0.8; ***B***, red line). ***D***, The number of SBE classes depended on the distance threshold applied to group SBEs. PKC^- and PKC^+ networks formed significantly fewer classes for low and intermediate distance thresholds. ***E***, Fraction of all SBEs of the *N*-most frequently occurring SBE classes. In PKC^- networks a significantly smaller number of pattern classes dominated the activity. Bars above the panel indicates the range of pairs with $p_{stt} < 0.01$ tested versus PKC^N.

diversity of propagation patterns. Instead pattern diversity was reduced and more similar to PKC^- patterns with respect to their intraclass similarity, although this was statistically significant only for low classification thresholds between 0.02 and 0.16 (correlation coefficient, 0.84–0.98; average number of classes resulting from classification of 100 SBEs with a threshold of 0.2: PKC^N, 59.3 ± 2.7; $N = 33$; PKC^-, 17.5 ± 2.8; $p_{stt} = 3.6*10^{-13}$; $N = 17$; PKC^+, 46.4 ± 8.0; $N = 8$). In PKC^- networks, SBE activity was dominated by a smaller number of pattern classes than in PKC^N and PKC^+ networks (Fig. 7*E*). On average, the five most frequent classes accounted for $89.1 \pm 2.8\%$ ($p_{stt} = 5.5*10^{-11}$ vs PKC^N) of the SBEs in PKC^- networks but accounted for only $44.5 \pm 3.5\%$ in PKC^N and $53.8 \pm 8.6\%$ in PKC^+ networks.

Clustering promotes spatial variability of SBE initiation

SBEs typically initiated locally in BIZs, here defined by the electrodes at which spikes assigned to a burst were detected first (Fig. 8*A*). With large MEAs that covered networks almost fully, we identified the position of such BIZs. In all networks, BIZs clustered spatially, indicating hot spots of SBE initiation, and had a propensity to be located at the network boundary (Fig. 8*B*). Consistent with the low diversity of SBE propagation patterns, BIZs were more clustered in PKC^- networks than in PKC^N and PKC^+ networks. BIZs alternated in eliciting SBE (Fig. 8*B*, right), with clusters of BIZs (hotspots) dominating SBE initiation in particular in PKC^- networks. In all network types, spiking activity increased in the vicinity (~1.5 mm) of the BIZ before SBE onset (Fig. 8*C*). Interestingly, in PKC^+ networks, activity could persist between SBEs in particular in the BIZ.

Influence of inhibition on spontaneous dynamics

The influence of inhibition in a network depends on the connectivity of inhibitory neurons and thus may differ in networks with different architecture. To test the influence of inhibition on spon-

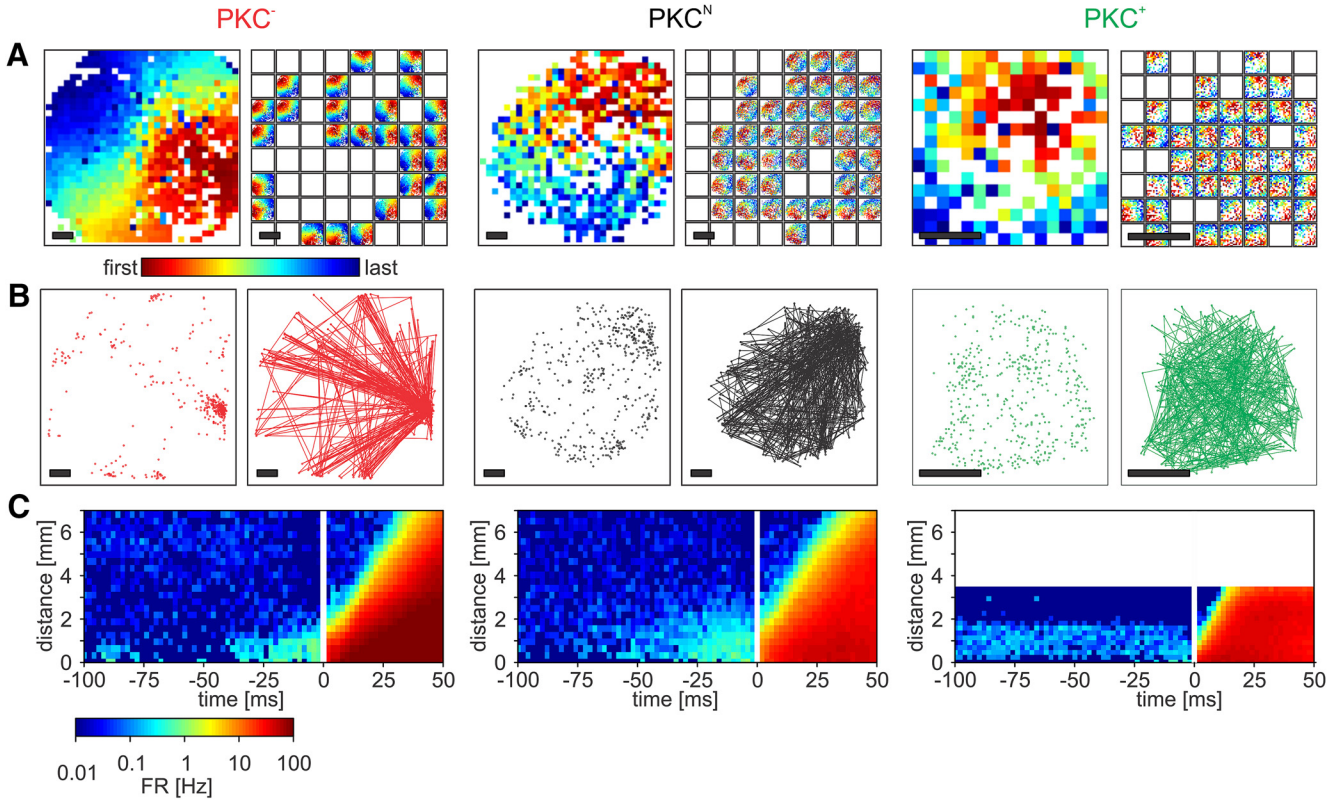

Figure 8. BIZs and network hotspots. ***A***, SBEs were typically elicited in local areas of the network and spread with a traveling wave front. Note the smoother wave fronts in PKC$^-$ and PKC$^+$ networks compared with those in PKC^N networks. In these recordings, the MEA covered most of the network. PKC$^-$ and PKC^N networks were recorded with 1000 electrodes PKC$^+$ networks were recorded with 256 electrodes. Color indicates rank order of the first spikes recorded for an SBE at a given electrode. Left, One sample pattern. Right, Samples of typical patterns placed according to their BIZ, regardless of their frequency of occurrence (downsampled to 8 × 8 tiles with 8 × 8 and 4 × 4 electrodes). ***B***, SBE initiation in the PKC$^-$ networks was typically dominated by few BIZs at the network boundary. Right, The trajectory depicts the temporal sequence of BIZs eliciting SBEs (300 SBEs) by connecting BIZ of successive SBEs. In PKC^N and PKC$^+$ networks, SBEs were elicited from many distributed and alternating BIZs. Scale bars: ***A***, ***B***, 100 μm. ***C***, Spatiotemporal firing-rate histogram relative to SBE onset (0 ms) and BIZ (0 mm). In all network types, activity accumulated within a distance of 1–2 mm to the BIZ before SBE onset (averages of 500 consecutive SBEs at 30 DIV).

taneous activity dynamics, we disinhibited networks with PTX applied at a concentration blocking ionotropic GABAergic transmission (10 μM; Krishek et al., 1996). PTX application increased spontaneous activity (AFRs) in all network types with the strongest effect in PKC$^-$ networks (Student's *t* test for paired samples: PKC^N, +119 ± 33%; $N = 18$; $p = 4.9*10^{-3}$; PKC$^-$, +496 ± 108%; $N = 18$; $p = 1.1*10^{-5}$; PKC$^+$, +88 ± 45%; $N = 8$; $p = 1.1*10^{-2}$; Fig. 9*A*). More detailed analysis showed that this was due to significantly stronger bursting (spikes/site) during SBEs (PKC^N, +980 ± 378%; $p = 5.1*10^{-4}$; PKC$^-$, +598 ± 96%; $p = 4.6*10^{-7}$; PKC$^+$, +724 ± 101%; $p = 0.069$; Fig. 9*B*). In a result counterintuitive to the expectation that increased excitability following disinhibition promotes SBE initiation, SBE rates significantly decreased in PKC^N and PKC$^+$ networks after adding PTX, and remained at the low baseline levels in PKC$^-$ networks (PKC^N, −62 ± 4%, $p = 2.7*10^{-5}$; PKC$^-$, −1 ± 12%; $p = 0.16$; PKC$^+$, −72 ± 6%; $p = 1.1*10^{-2}$; Fig. 9*C*).

These observations suggest that burst strength-dependent network depression and recovery could limit SBE rates. Lower activity, more negative resting $V_{m,}$, and the pronounced increase of SBE strength upon disinhibition in PKC$^-$ networks could result from increased or more effective inhibition compared with PKC^N networks. This then would also predict that their excitability should be lower. To investigate whether PKC$^-$ networks were limited by reduced excitability, we stimulated PKC$^-$ and PKC^N networks electrically.

PKC$^-$ networks support high activity levels

To test whether PKC$^-$ networks can support higher SBE rates, we stimulated a separate set of networks electrically with interstimulus intervals of either 6, 4, or 2 s at alternating stimulation sites, corresponding to the range of spontaneous SBE activation intervals and the alternating BIZs in PKC^N networks. In PKC$^-$ networks, electrical stimulation significantly increased AFRs (6 s interval +583 ± 245%, $p = 0.030$; 4 s interval +757 ± 332%, $p = 0.023$; 2 s interval +859 ± 344%, $p = 0.011$; $N = 3$; mean ± SEM; Student's *t* test for paired samples; Fig. 9*D*) and SBE rates (6 s interval, +762 ± 327%; $p = 6.1*10^{-4}$; 4 s interval, +1117 ± 466%; $p = 6.1*10^{-4}$; 2 s interval, +1978 ± 755%; $p = 9.6*10^{-4}$; spontaneous and evoked SBEs; Fig. 9*F*) beyond the level of spontaneous activity in PKC^N networks. Moreover, PKC$^-$ networks showed almost complete entrainment of the SBE activity to the stimulation with very high response probability (evoked responses within 100 ms for 91.3, 87.6, and 81.4% of the stimuli given in series of 1200 stimuli at 6, 4, and 2 s intervals, respectively; $N = 4$) and highly reproducible propagation patterns (similar to spontaneous propagation patterns). Stimulation only slightly increased gross average activity levels in PKC^N networks (6 s interval, +31 ± 6%; 4 s interval, +44 ± 17%; 2 s interval, +73 ± 25%; differences were not statistically significant; $N = 3$; Fig. 9*D*) and SBE rate (6 s interval, +76 ± 39%; 4 s interval, +95 ± 57%; 2 s interval, +194 ± 112%; differences were not statistically significant; Fig. 9*F*). PKC^N networks were less re-

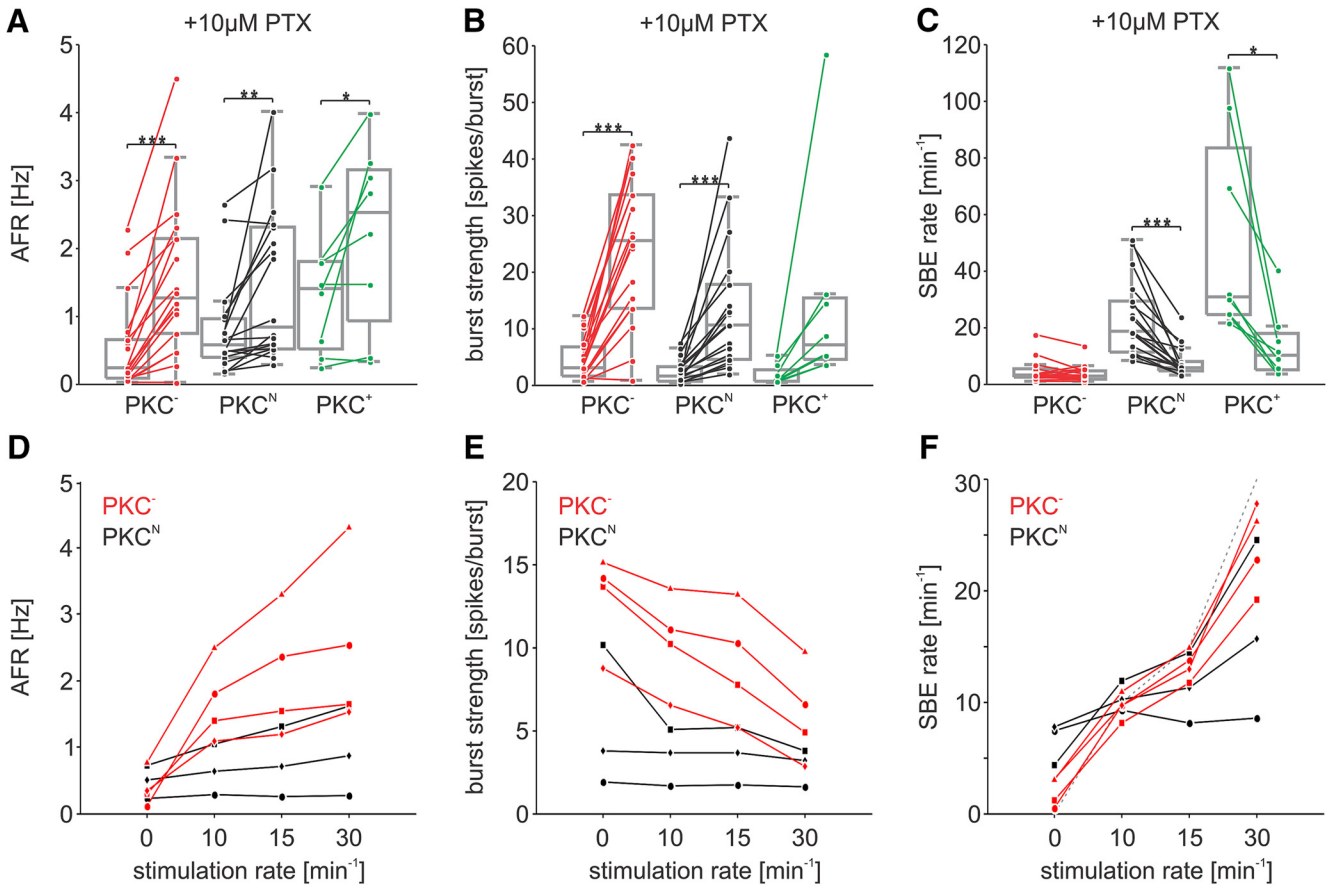

Figure 9. Effects of disinhibition and electrical stimulation. ***A–C***, Blocking GABA receptors (10 μM PTX) in PKC^N networks produced stronger bursts at the expense of lowered SBE rates. AFRs significantly increased despite of this trade-off. PTX application likewise increased SBE strength in PKC$^-$ networks did not affect SBE rates. In consequence, AFRs significantly increased. ***D–F***, To assess the maximal activity level supported by a network, we electrically stimulated at alternating sites. PKC$^-$ networks were highly responsive, producing SBE rates close to the rate of stimulation (dashed line). Higher SBE rates (spontaneous or evoked) were at the cost of weaker bursts with fewer APs per site and SBE but still resulted in significantly increased AFRs. PKC^N networks were less responsive to stimulation than PKC$^-$ networks and showed no significant increase of AFRs. Boxplots show median, 25th, and 75th percentiles and minimal and maximal values (excluding outliers). $^{**}p = 0.01$; $^{***}p = 0.001$.

sponsive to stimulation (response probabilities: 6 s interval, 48.8%; 4 s interval, 48.4%; 2 s interval, 45.6%) and responses were much more variable. Additional SBEs started spontaneously between stimuli. Eliciting additional SBEs by stimulation reduced SBE strength in both network types but differences between control and stimulation sessions were not statistically significant for PKC^N (PKC^N: 6 s interval, $-22 \pm 12\%$; 4 s interval, $-21 \pm 12\%$; 2 s interval, $-32 \pm 13\%$; PKC$^-$: 6 s interval, $-21 \pm 3\%$; $p = 0.009$; 4 s interval, $-31 \pm 5\%$; $p = 0.018$; 2 s interval, $-55 \pm 6\%$; $p = 0.003$; Fig. 9*E*). In summary, SBE rates in PKC$^-$ networks were neither limited by their capacity to sustain higher rates nor by GABAergic inhibition. Electrically driven activity showed a dynamical trade-off between SBE rate and SBE strength.

Removal of PKC modulators after chronic exposure

To identify direct effects of the PKC modulators on the network activity, we replaced the medium with fresh drug-free medium after 4 weeks in all three PKC activity conditions (Fig. 10). Washout-induced changes of burst activity were similar in all groups. Relative differences in spontaneous activity between PKC activity conditions were preserved for ≥3 DIV after drug removal. This supports the idea that the findings above were related to changes in network structure rather than to direct drug effects.

Discussion

Computational network models suggest that clustered connectivity is beneficial for generation, maintenance (Kaiser and Hilgetag, 2010; Stetter et al., 2012; Klinshov et al., 2014), and variability of spontaneous activity dynamics in neuronal networks (Litwin-Kumar and Doiron, 2012). We addressed this issue in cortical networks *in vitro* in which we manipulated the degree of clustering and neurite bundling.

Manipulating mesoscale network architecture by PKC modulation

Networks *in vitro* establish community structures (Girvan and Newman, 2002; Sporns, 2013) exhibiting local neuron clusters with strongly entangled neurites, neurite bundles interconnecting clusters, and long-range axons (Kriegstein and Dichter, 1983; Shefi et al., 2002; Bettencourt et al., 2007; Stetter et al., 2012). We manipulated this architecture by modulating PKC activity. The control of cell migration and neurite outgrowth by PKC has been discussed previously (Itoh et al., 1989; Dent and Meiri, 1998; Kumada and Komuro, 2004; Larsson, 2006; Metzger, 2010). Diminishing PKC activity during network development produced remarkably uniform networks with more randomly distributed somata and less fasciculated neurites than in PKC^N networks. The opposite effects resulted from stimula-

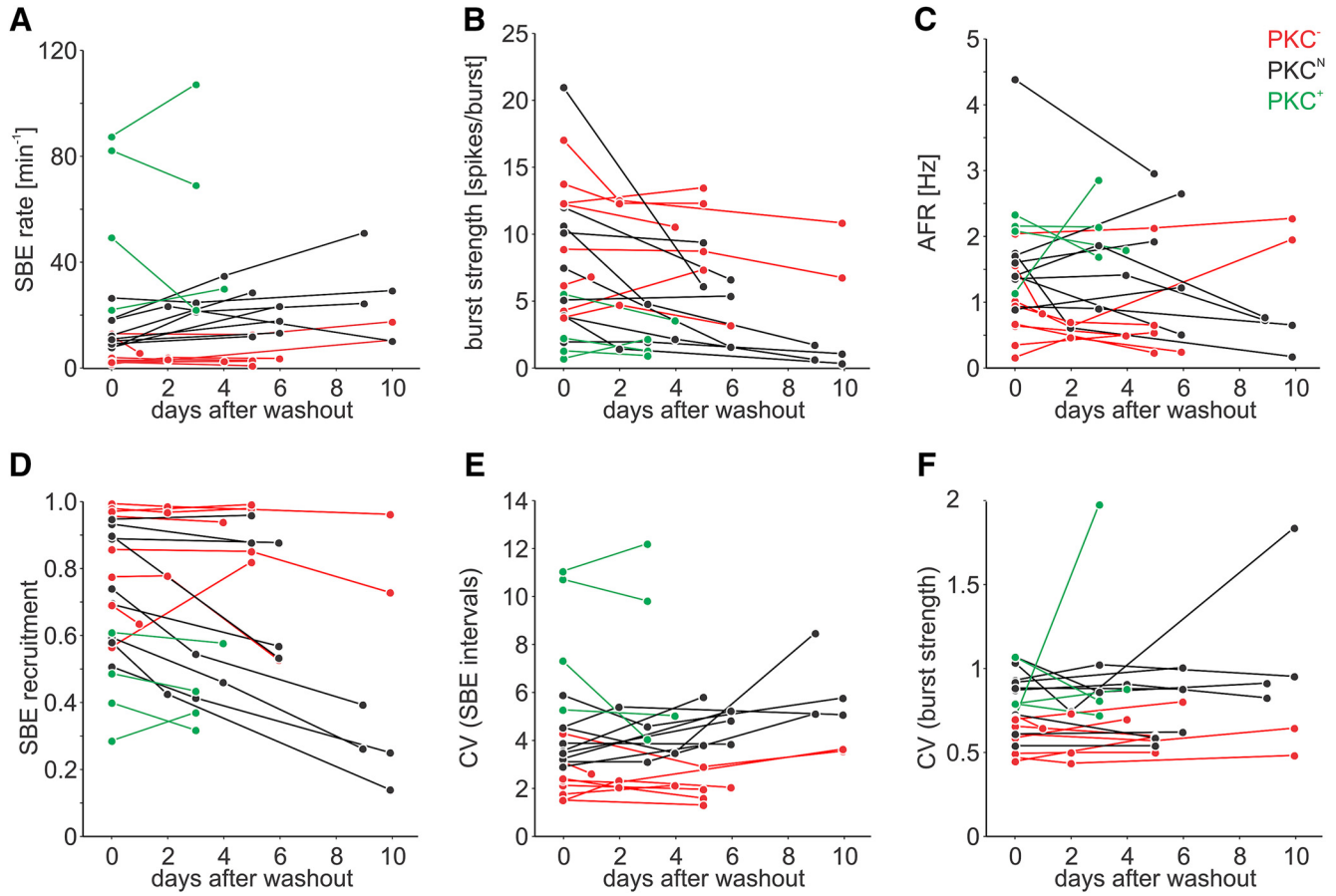

Figure 10. Effects of drug washout following chronic treatment. ***A–F***, Complete medium exchange with fresh drug-free medium after 30 d of chronic treatment with PKC modulators produced no systematic changes of the activity dynamics. Changes in PKC^N networks indicate an effect of the washout itself, likely due to the strong perturbation or the replacement with fresh medium. Changes in PKC-modulated networks were in the same range or smaller than those in PKC^N networks. See Figure 6 for further details.

tion of PKC, which promoted spatial aggregation of somata and local neurite sprouting within regularly spaced and well delineated clusters.

As with cerebellar Purkinje cells (Metzger, 2010), PKC inhibition increased neurite fields and neurite densities. This presumably increases the probability of a synaptic connection between any pair of neurons, predicting increased availability of long-range connections. Conversely, lower neurite and, in particular, lower axon densities in PKC^+ networks should reduce long-range connectivity. Pronounced tangles of neurites within clusters, in turn, likely promote highly recurrent local connectivity. In addition, axon bundles formed mainly between neighboring clusters.

We therefore hypothesize that diminished PKC activity shifted the network toward uniform connectivity, whereas increasing PKC activity promoted recurrent connectivity within and convergent connectivity between local clusters at the expense of long-range connectivity.

Mesoscale network architecture and synaptic dynamics

Anatomical analyses *in vivo* showed that statistically approximately a quarter of the contact sites between axon and dendrites are realized as functional connections (Stepanyants et al., 2002). Neurite architecture thus is a strong determinant of the realized synaptic connectivity. In our networks, synapses were indeed more uniformly distributed in PKC^- networks. Based on these observations and reports that the strength of synapses inversely scales with their number *in vitro* (Wilson et al., 2007) and *in vivo* (Turrigiano, 2008), smaller average EPSP amplitudes in PKC^- networks might be explained by the higher neurite density resulting in more synaptic connections. Although PKC has been implicated in synaptic plasticity (Saito and Shirai, 2002; Boehm et al., 2006), it is apparently not essential for activity-dependent synaptic plasticity due to other functionally redundant kinases (Wang and Kelly, 1996; Herring and Nicoll, 2016). If so, neurons should retain activity-dependent synaptic plasticity even with reduced PKC activity.

Large EPSP amplitudes in neurons associated with clusters are consistent with findings by Cohen et al. (2008) that in isolated clusters with <10 neurons, the stimulation of single neurons is sufficient to activate the entire ensemble while this is not possible in larger networks. EPSP amplitudes measured in neurons outside of clusters were indeed comparable across conditions, suggesting that their effective synaptic weights were not determined by the respective overall changes in network structure but reflected their local network embedding.

The larger EPSPs in clusters could also be explained by a higher propensity for multiple synaptic contacts between neuron pairs and the highly correlated presynaptic firing attributed to clusters (Helias et al., 2014). The precise synchrony among such connections, however, makes it impossible to distinguish between unitary EPSPs from single EPSPs and compound EPSPs from sister release sites.

Clustering promotes spontaneous SBE generation

V_m fluctuations strongly determine neuronal firing rates (Kuhn et al., 2004), which in a recurrent network translate back again into neuronal input statistics. Giugliano et al. (2004) hypothesized that SBE initiation is a threshold-gated process following activity integration on the network level analogous to the AP generation in neurons. Network architectures that increase background firing-rate fluctuations should thus promote SBE initiation. Along with larger EPSPs and higher EPSP frequencies, average V_m and V_m fluctuations increased with the degree of clustering in networks. Neurons consequently were more likely to reach the spiking threshold, which can be sufficient to activate an entire local cluster (Cohen et al., 2008). Fasciculation of axons that extend from clusters conveys highly correlated output to common target clusters, promoting focused long-range excitation. Neuronal clusters could thus act as local amplifiers or relay stations that promote generation of spontaneous activity and reliable transmission of activity within a network. Consistent with this, SBE rates significantly increased with the degree of clustering in networks. Furthermore, SBEs were elicited at widely distributed sites in clustered networks, suggesting that many local subnetworks exist that trigger SBEs. PKC$^-$ networks typically had few hotspots of SBE initiation. We propose that diminished neurite fasciculation fostered divergent rather than convergent connectivity patterns in these networks, reducing correlated input. Interestingly, hotspots were mostly located at the network boundary, which was most prominent in more uniform PKC$^-$ networks. In agreement with Gritsun et al. (2012), the boundary may enforce inward connections, thus promoting recurrent and convergent connectivity. Clusters may introduce additional BIZs by pronounced locally recurrent connectivity.

How changes in the network architecture affect overall inhibition levels and activity dynamics is difficult to predict. In PKC$^-$ networks excitation–inhibition balance could be more homogeneous than in clustered networks, where this could vary locally. This would introduce hot (and cold) spots that could further contribute to SBE initiation. Although recent studies find that homeostatic synaptic plasticity or spike-frequency adaptation could compensate for local excitation–inhibition imbalance (Barral and D Reyes, 2016; Landau et al., 2016), it is not clear whether this would fully flatten the excitation–inhibition landscape.

Global versus local synchrony

SBEs dominated in all networks, regardless of their particular mesoscale structure. However, SBE rate modulations and the occurrence of super bursts (Wagenaar et al., 2006b) increased with the degree of clustering and neurite fasciculation, which is consistent with network simulations showing that clustered topologies promote firing-rate variability (Litwin-Kumar and Doiron, 2012). In PKC$^-$ networks, activity reliably recruited most neurons once SBEs were initiated. In the strongly clustered PKC$^+$ networks, however, SBEs often remained confined to local network areas, as was observed in heavily clustered networks forming without adhesive growth substrates (Teller et al., 2014). We suggest that strong local dynamics in clusters and weak long-distance coupling entails global desynchronization analogous to effects described for weakly coupled oscillators (Strogatz and Mirollo, 1991; Park et al., 2006). Global synchrony thus should depend on the balance between local and global connectivity. Moderately clustered PKC^N networks were optimal in terms of allowing high SBE rates conjointly with strong network recruitment in SBEs and seem to possess sufficient recurrent connectivity to sustain activity as well as sufficient long-range connectivity to recruit distant parts of the network.

SBE initiation: a buildup or release process?

The rate of SBE succession may depend on recovery from synaptic depression and a buildup process that involves the amplification of activity in recurrent networks beyond a critical threshold (Tabak et al., 2010). To gain insight into the underlying mechanism, we tested networks by disinhibition and electrical stimulation. As described earlier (Weihberger et al., 2013), disinhibition only slightly increased overall spontaneous activity levels in PKC^N networks, since longer bursts were counterbalanced by lower SBE rates. This trade-off suggests that PKC^N networks operate within a regime of activity that exploits most resources. In agreement with this, overall activity levels could not be increased much by external stimulation. In PKC$^-$ networks, amplified bursting through disinhibition was not balanced by lower SBE rates, suggesting rate limitation by the initiation process rather than by synaptic resources. Consistent with this assumption, electrical stimulation significantly increased activity levels and SBE rates.

Clustering promotes richness of activity patterns

In accordance with Soriano et al. (2008), we found discrete network areas that had a high propensity to trigger SBEs. These BIZs were frequent and widely distributed in clustered networks and less abundant in homogenous PKC$^-$ networks, which is consistent with the idea that convergent and recurrent connectivity patterns promote burst initiation. In all networks, SBEs spread with approximately circular wave fronts. Interestingly, PKC$^+$ networks displayed more regular wave fronts than PKC^N networks, rather similar to those observed in PKC$^-$ networks. One could argue that this is because regular spacing of clusters in PKC$^+$ networks likewise introduces uniformity at the mesoscale level. Since the local direction of propagation depended mainly on the BIZ location, distributed BIZs in clustered networks fostered a rich repertoire of different spatiotemporal propagation patterns.

Conclusion

We showed that modulation of PKC during network development can change the balance between locally clustered and long-range connectivity. Consistent with network simulations, our data indicate that clustering promotes local activity generation but leads to reduced global synchrony. Intriguingly, the richness of structure and activity patterns in PKC^N networks are suggestive of small-world and scale-free topologies with their computational advantages. We propose that the coevolution of spontaneous activity levels, richness of activity patterns, and community network structure reflects a fundamental principle of neuronal self-organization.

References

Altwegg-Boussac T, Chavez M, Mahon S, Charpier S (2014) Excitability and responsiveness of rat barrel cortex neurons in the presence and absence of spontaneous synaptic activity in vivo. J Physiol 592:3577–3595. CrossRef Medline

Audesirk G, Cabell L, Kern M (1997) Modulation of neurite branching by protein phosphorylation in cultured rat hippocampal neurons. Brain Res Dev Brain Res 102:247–260. CrossRef Medline

Barral J, D Reyes A (2016) Synaptic scaling rule preserves excitatory-inhibitory balance and salient neuronal network dynamics. Nat Neurosci 19:1690–1696. CrossRef Medline

Bettencourt LM, Stephens GJ, Ham MI, Gross GW (2007) Functional structure of cortical neuronal networks grown in vitro. Phys Rev E Stat Nonlin Soft Matter Phys 75:021915. CrossRef Medline

Biffi E, Regalia G, Menegon A, Ferrigno G, Pedrocchi A (2013) The influence of neuronal density and maturation on network activity of hippocampal cell cultures: a methodological study. PLoS One 8:e83899. CrossRef Medline

Boehm J, Kang MG, Johnson RC, Esteban J, Huganir RL, Malinow R (2006) Synaptic incorporation of AMPA receptors during LTP is controlled by a PKC phosphorylation site on GluR1. Neuron 51:213–225. CrossRef Medline

Bosking WH, Zhang Y, Schofield B, Fitzpatrick D (1997) Orientation selectivity and the arrangement of horizontal connections in tree shrew striate cortex. J Neurosci 17:2112–2127. Medline

Chavane F, Sharon D, Jancke D, Marre O, Frégnac Y, Grinvald A (2011) Lateral spread of orientation selectivity in V1 is controlled by intracortical cooperativity. Front Syst Neurosci 5:4. CrossRef Medline

Clark PJ, Evans FC (1954) Distance to nearest neighbor as a measure of spatial relationships in populations. Ecol Soc Am Stable 35:445–453.

Cohen E, Ivenshitz M, Amor-Baroukh V, Greenberger V, Segal M (2008) Determinants of spontaneous activity in networks of cultured hippocampus. Brain Res 1235:21–30. CrossRef Medline

Dent EW, Meiri KF (1998) Distribution of phosphorylated GAP-43 (neuromodulin) in growth cones directly reflects growth cone behavior. J Neurobiol 35:287–299. CrossRef Medline

Egert U, Knott T, Schwarz C, Nawrot M, Brandt A, Rotter S, Diesmann M (2002) MEA-Tools: an open source toolbox for the analysis of multi-electrode data with MATLAB. J Neurosci Methods 117:33–42. CrossRef Medline

Galli-Resta L, Novelli E, Kryger Z, Jacobs GH, Reese BE (1999) Modelling the mosaic organization of rod and cone photoreceptors with a minimal-spacing rule. Eur J Neurosci 11:1461–1469. CrossRef Medline

Girvan M, Newman ME (2002) Community structure in social and biological networks. Proc Natl Acad Sci U S A 99:7821–7826. CrossRef Medline

Giugliano M, Darbon P, Arsiero M, Lüscher H-R, Streit J (2004) Single-neuron discharge properties and network activity in dissociated cultures of neocortex. J Neurophysiol 92:977–996. Medline

Golshani P, Gonçalves JT, Khoshkhoo S, Mostany R, Smirnakis S, Portera-Cailliau C (2009) Internally mediated developmental desynchronization of neocortical network activity. J Neurosci 29:10890–10899. CrossRef Medline

Gritsun TA, le Feber J, Rutten WL (2012) Growth dynamics explain the development of spatiotemporal burst activity of young cultured neuronal networks in detail. PLoS One 7:e43352. CrossRef Medline

Gundlfinger A, Kapfhammer JP, Kruse F, Leitges M, Metzger F (2003) Different regulation of Purkinje cell dendritic development in cerebellar slice cultures by protein kinase Calpha and -beta. J Neurobiol 57:95–109. CrossRef Medline

Helias M, Tetzlaff T, Diesmann M (2014) The correlation structure of local neuronal networks intrinsically results from recurrent dynamics. PLoS Comput Biol 10:e1003428. CrossRef Medline

Herring BE, Nicoll RA (2016) Long-term potentiation: from CaMKII to AMPA receptor trafficking. Annu Rev Physiol 78:351–365. CrossRef Medline

Itoh K, Asou H, Ikarashi Y, Maruyama Y (1989) Morphological changes and neural cell adhesion molecule expression in mouse cerebrum primary cultures following long-term exposure to phorbol ester. Neurosci Res 6:350–357. CrossRef Medline

Kaiser M, Hilgetag CC (2010) Optimal hierarchical modular topologies for producing limited sustained activation of neural networks. Front Neuroinform 4:8. CrossRef Medline

Katz LC, Shatz CJ (1996) Synaptic activity and the construction of cortical circuits. Science 274:1133–1138. CrossRef Medline

Kilb W, Kirischuk S, Luhmann HJ (2011) Electrical activity patterns and the functional maturation of the neocortex. Eur J Neurosci 34:1677–1686. CrossRef Medline

Klinshov VV, Teramae JN, Nekorkin VI, Fukai T (2014) Dense neuron clustering explains connectivity statistics in cortical microcircuits. PLoS One 9:e94292. CrossRef Medline

Kriegstein AR, Dichter MA (1983) Morphological classification of rat cortical neurons in cell culture. J Neurosci 3:1634–1647. Medline

Krishek BJ, Moss SJ, Smart TG (1996) A functional comparison of the antagonists bicuculline and picrotoxin at recombinant GABAA receptors. Neuropharmacology 35:1289–1298. CrossRef Medline

Kuhn A, Aertsen A, Rotter S (2004) Neuronal integration of synaptic input in the fluctuation-driven regime. J Neurosci 24:2345–2356. CrossRef Medline

Kumada T, Komuro H (2004) Completion of neuronal migration regulated by loss of Ca(2+) transients. Proc Natl Acad Sci U S A 101:8479–8484. CrossRef Medline

Landau ID, Egger R, Dercksen VJ, Oberlaender M, Sompolinsky H (2016) The impact of structural heterogeneity on excitation-inhibition balance in cortical networks. Neuron 92:1106–1121. CrossRef Medline

Larsson C (2006) Protein kinase C and the regulation of the actin cytoskeleton. Cell Signal 18:276–284. CrossRef Medline

Litwin-Kumar A, Doiron B (2012) Slow dynamics and high variability in balanced cortical networks with clustered connections. Nat Neurosci 15:1498–1505. CrossRef Medline

Liu X, Zhu XH, Qiu P, Chen W (2012) A correlation-matrix-based hierarchical clustering method for functional connectivity analysis. J Neurosci Methods 211:94–102. CrossRef Medline

Logothetis NK, Murayama Y, Augath M, Steffen T, Werner J, Oeltermann A (2009) How not to study spontaneous activity. Neuroimage 45:1080–1089. CrossRef Medline

Marom S, Shahaf G (2002) Development, learning and memory in large random networks of cortical neurons: lessons beyond anatomy. Q Rev Biophys 35:63–87. Medline

Meier R, Egert U, Aertsen A, Nawrot MP (2008) FIND—a unified framework for neural data analysis. Neural Netw 21:1085–1093. CrossRef Medline

Metzger F (2010) Molecular and cellular control of dendrite maturation during brain development. Curr Mol Pharmacol 3:1–11. CrossRef Medline

Park K, Lai YC, Gupte S, Kim JW (2006) Synchronization in complex networks with a modular structure. Chaos 16:015105. CrossRef Medline

Quinlan EM, Halpain S (1996) Emergence of activity-dependent, bidirectional control of microtubule-associated protein MAP2 phosphorylation during postnatal development. J Neurosci 16:7627–7637. Medline

Ringach DL (2009) Spontaneous and driven cortical activity: implications for computation. Curr Opin Neurobiol 19:439–444. CrossRef Medline

Robert F, Cloix JF, Hevor T (2012) Ultrastructural characterization of rat neurons in primary culture. Neuroscience 200:248–260. CrossRef Medline

Ruthazer ES, Stryker MP (1996) The role of activity in the development of long-range horizontal connections in area 17 of the ferret. J Neurosci 16:7253–7269. Medline

Saito N, Shirai Y (2002) Protein kinase C gamma (PKC gamma): function of neuron specific isotype. J Biochem 132:683–687. CrossRef Medline

Sanchez-Vives MV, McCormick DA (2000) Cellular and network mechanisms of rhythmic recurrent activity in neocortex. Nat Neurosci 3:1027–1034. CrossRef Medline

Sato TK, Nauhaus I, Carandini M (2012) Traveling waves in visual cortex. Neuron 75:218–229. CrossRef Medline

Schrenk K, Kapfhammer JP, Metzger F (2002) Altered dendritic development of cerebellar Purkinje cells in slice cultures from protein kinase Cgamma-deficient mice. Neuroscience 110:675–689. CrossRef Medline

Segev R, Benveniste M, Shapira Y, Ben-Jacob E (2003) Formation of electrically active clusterized neural networks. Phys Rev Lett 90:168101. CrossRef Medline

Shahaf G, Marom S (2001) Learning in networks of cortical neurons. J Neurosci 21:8782–8788. Medline

Shahaf G, Eytan D, Gal A, Kermany E, Lyakhov V, Zrenner C, Marom S (2008) Order-based representation in random networks of cortical neurons. PLoS Comput Biol 4:e1000228. CrossRef Medline

Shatz CJ (1996) Emergence of order in visual system development. Proc Natl Acad Sci U S A 93:602–608. CrossRef Medline

Shefi O, Golding I, Segev R, Ben-Jacob E, Ayali A (2002) Morphological characterization of in vitro neuronal networks. Phys Rev E Stat Nonlin Soft Matter Phys 66:021905. CrossRef Medline

Sholl DA (1953) Dendritic organization in the neurons of the visual and motor cortices of the cat. J Anat 87:387–406. Medline

Soriano J, Rodríguez Martínez M, Tlusty T, Moses E (2008) Development of input connections in neural cultures. Proc Natl Acad Sci U S A 105:13758–13763. CrossRef Medline

Sporns O (2013) Structure and function of complex brain networks. Dialogues Clin Neurosci 15:247–262. Medline

Stepanyants A, Hof PR, Chklovskii DB (2002) Geometry and structural plasticity of synaptic connectivity. Neuron 34:275–288. CrossRef Medline

Stetter O, Battaglia D, Soriano J, Geisel T (2012) Model-free reconstruction of excitatory neuronal connectivity from calcium imaging signals. PLoS Comput Biol 8:e1002653. CrossRef Medline

Strogatz SH, Mirollo RE (1991) Stability of incoherence in a population of coupled oscillators. J Stat Phys 63:613–635. CrossRef

Tabak J, Mascagni M, Bertram R (2010) Mechanism for the universal pattern of activity in developing neuronal networks. J Neurophysiol 103: 2208–2221. CrossRef Medline

Teller S, Granell C, De Domenico M, Soriano J, Gómez S, Arenas A (2014) Emergence of assortative mixing between clusters of cultured neurons. PLoS Comput Biol 10:e1003796. CrossRef Medline

Turrigiano GG (2008) The self-tuning neuron: synaptic scaling of excitatory synapses. Cell 135:422–435. CrossRef Medline

van Pelt J, Wolters PS, Corner MA, Rutten WL, Ramakers GJ (2004) Long-term characterization of firing dynamics of spontaneous bursts in cultured neural networks. IEEE Trans Biomed Eng 51:2051–2062. CrossRef Medline

Voges N, Guijarro C, Aertsen A, Rotter S (2010) Models of cortical networks with long-range patchy projections. J Comput Neurosci 28:137–154. CrossRef Medline

Wagenaar DA, Potter SM (2004) A versatile all-channel stimulator for electrode arrays, with real-time control. J Neural Eng 1:39–45. CrossRef Medline

Wagenaar DA, Pine J, Potter SM (2006a) An extremely rich repertoire of bursting patterns during the development of cortical cultures. BMC Neurosci 7:11. CrossRef Medline

Wagenaar DA, Nadasdy Z, Potter SM (2006b) Persistent dynamic attractors in activity patterns of cultured neuronal networks. Phys Rev E Stat Nonlin Soft Matter Phys 73:051907. CrossRef Medline

Wang JH, Kelly PT (1996) The balance between postsynaptic Ca(2+)-dependent protein kinase and phosphatase activities controlling synaptic strength. Learn Mem 3:170–181. CrossRef Medline

Weihberger O, Okujeni S, Mikkonen JE, Egert U (2013) Quantitative examination of stimulus-response relations in cortical networks in vitro. J Neurophysiol 109:1764–1774. CrossRef Medline

Wilson NR, Ty MT, Ingber DE, Sur M, Liu G (2007) Synaptic reorganization in scaled networks of controlled size. J Neurosci 27:13581–13589. CrossRef Medline

Wu JY, Huang X, Zhang C (2008) Propagating waves of activity in the neocortex: what they are, what they do. Neuroscientist 14:487–502. CrossRef Medline

Yanagawa T, Mogi K (2009) Analysis of ongoing dynamics in neural networks. Neurosci Res 64:177–184. CrossRef Medline